Quantifying fault interpretation uncertainties and their impact on fault seal and seismic hazard analysis

Billy J. Andrews[1*]; Zoë K. Mildon[1]; Christopher A. L. Jackson[2]; Clare E. Bond[3]

1) School of Geography, Earth and Environmental Sciences, University of Plymouth, Drake Circus, Plymouth, PL4 8AA, UK
2) Department of Earth Science & Engineering, Imperial College, Prince Consort Road, London, SW7 2BP, UK
3) Department of Geology and Geophysics, School of Geoscience, Meston Building, Aberdeen University, Aberdeen, AB24 3UE, UK

billy.andrews@plymouth.ac.uk Tel: +44 1752 600 600

Zoe.mildon@plymouth.ac.uk

c.jackson@imperial.ac.uk

clare.bond@abdn.ac.uk

Key words: Bias, Seismic reflection, Displacement analysis, Faults

Acknowledgements

We would like to thank DugInsight for the provision of an academic license for their software package.

This work was supported by a UKRI Future Leaders Fellowship MR/T041994/1.

Abstract

Fault-horizon cut-off data extracted from seismic reflection datasets are used to study the geometry, displacement distribution, and growth history of normal faults. Our study assesses the influence of three fault interpretation factors (repeatability, measurement obliquity, and cut-off type) on derived fault properties. We investigate uncertainties in throw, heave, displacement, and dip, extracted from continuous and discontinuous cut-offs along multiple horizons across four sub-linear faults in the Chandon-3D seismic cube, located offshore NW Australia. Mean differences between repeated interpretations are ~±10% for throw and 13-23% for heave, with greater uncertainties observed locally (e.g., in areas of structural complexity). Measurement obliquity, where cut-offs are interpreted along non-perpendicular transects to fault strike, introduces uncertainty depending on the degree of obliquity (particularly when >20˚), horizon, fault, and the fault property being measured. Obliquity related uncertainties were found to not decrease the repeatability of the derived fault parameters, with the seismic image data found to have a greater influence. For both the aforementioned interpretation factors, continuous cut-offs generally exhibit greater uncertainties compared to discontinuous cut-offs. Our findings indicate that obliquity and repeatability have a limited impact on fault transmissivity calculations but may significantly affect fault-based seismic hazard assessment.

1 Introduction

The measurement of horizon-fault cut-offs from seismic reflection datasets enables extraction of key fault properties such as heave, throw and fault dip. Analysis of these properties have to advanced our understanding of fault geometry and evolution (e.g., Nicol et al., 2005; Jackson and Rotevatn, 2013; Pan et al., 2021; Roche et al., 2021; Rodríguez-Salgado et al., 2023), strain rate and its evolution in active and inactive rift systems (e.g., Meyer et al., 2002; Cowie et al., 2005; Marsh et al., 2010); and fluid-flow properties of faults within hydrocarbon and/or CO_2 reservoirs (e.g.,Yielding, 2002; Gibson and Bentham, 2003; Yielding et al., 2011; Miocic et al., 2014). The use of horizon-fault cut-off data, combined with well data, is routinely used to infer the sealing potential of faults cutting these reservoirs. This is of particular importance for CO_2 storage projects (Klusman, 2003; Amonette et al., 2010), where schemes are required to ensure at least 99% of injected CO_2 must remain within the target reservoir for >1000 years (IPCC, 2005). Fault cut-off data can also be used to infer key properties to feed into fault based seismic hazard assessment (e.g., fault dip, geological slip rate) (Nicol et al., 2005). Nucular waste disposal sites require geologically stable subsurface locations, and hence must be subject to detailed seismic hazard assessment (Fenton et al., 2006; Connor et al., 2009; Mörner, 2013). Where 3D seismic data is involved in this assessment, any uncertainty in cut-off data could lead to uncertainties in the expected hazard at the site and therefore its suitability for storing nuclear waste. It is therefore imperitive to have confidence in conclusions drawn from the analysis of fault properties extracted from seismic reflection datasets and therefore, the uncertainties and biases associated with extraction of underpinning data.

Uncertainties can be broadly classified as objective and subjective (Frodeman, 1995; Tannert et al., 2007; Bond, 2015). Objective uncertainty, also known as “stochastic uncertainty”, relates to the methods used for data acquisition, analysis, or interpretation of the raw data (Tannert et al., 2007; Pérez-Díaz et al., 2020). In the case of seismic reflection data, these include the velocity model used for the conversion between two-way-time to depth (Schaaf and Bond, 2019; Faleide et al., 2021), the effect of compaction of fault properties (Taylor et al., 2008), the spacing of picks during data extraction (Michie et al., 2021), and whether the throw across a given fault exceeds or falls below the limit of separability (Brown, 2011; Osagiede et al., 2014). Subjective uncertainties pertain to biases and variability in results caused by the individual analysing the data (Tannert et al., 2007), these include the geological interpretation and it’s repeatability. Repeatability, which is the ability to replicate the data and interpretations of a study, is recognised as a crucial aspect of any experiment (e.g., Goodman, 2016). Geology, in particular, is susceptible to subjective uncertainty due to incomplete datasets and the lack of consensus within the research community regarding key concepts and research methods (Frodeman, 1995; Bond, 2015; Pérez-Díaz et al., 2020; Steventon et al., 2022; Magee et al., 2023; Robledo Carvajal et al., 2023). For seismic reflection datasets, subjective uncertainties can lead to multiple interpretations being drawn from the same seismic image (e.g., Bond et al., 2007; Alcalde et al., 2017). Previous work has suggested that fault properties extracted from seismic reflection data should have an error associated with then of between ±5% (Magee and Jackson, 2020a) and ±10% (Magee et al., 2023), however, no parametric studies have been undertaken to date to test these essentially qualitative values.

Motivated by the discussion above, this paper addresses three previously understudied uncertainties in fault interpretation using seismic reflecton images: repeatability; measurement obliquity; and interpreted cut-off type. We examine the impact of the related uncertainties on the following fault properties: throw, heave, dip, and displacement. Finally, we discuss the implications of our findings for understanding fault transmissibility and seismic hazard assessment.

1.1 Expected sources of uncertainty in fault interpretation

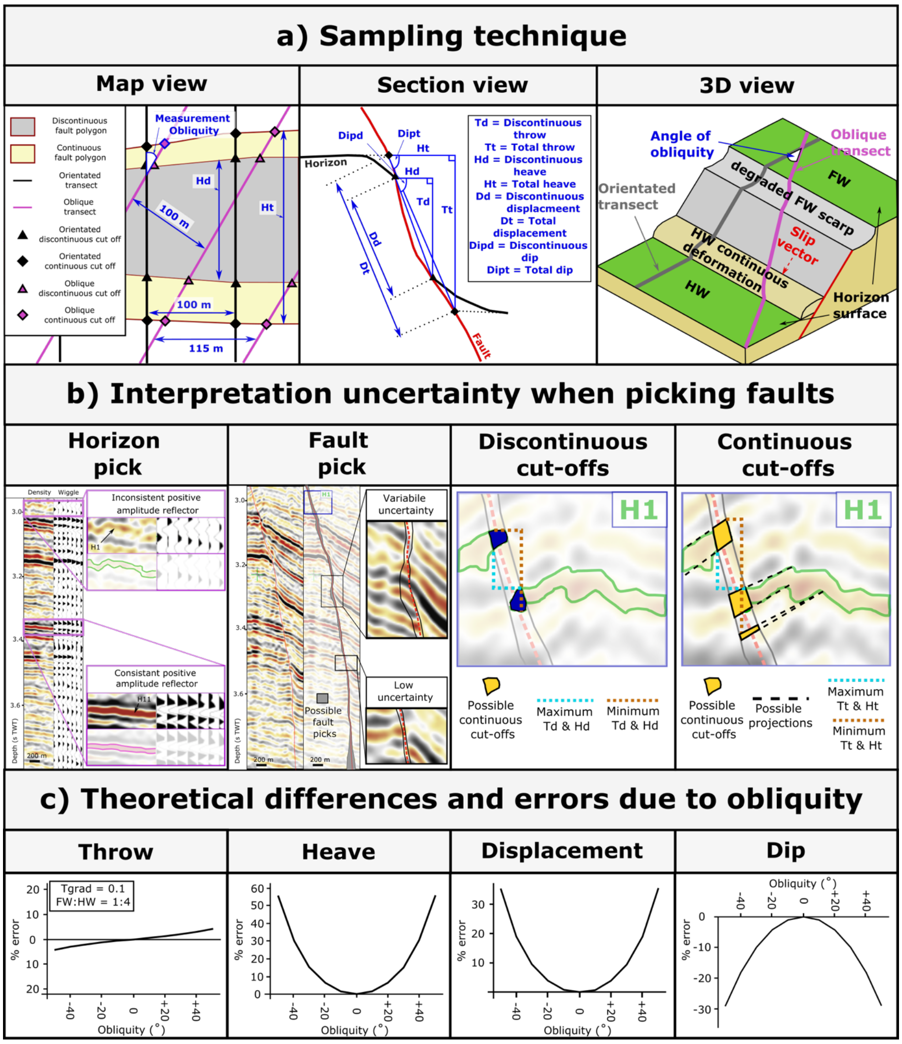

Figure 1: Sample strategy and theoretical impact of obliquity on extracted fault parameters: a) sample strategy and extracted parameters showing in map and section and 3D views. Discontinuous and continuous fault polygons represent the horizon gap created by a fault, extending between the hanging wall and footwall for discontinuous and continuous cut-offs, respectively; b) examples of expected interpretation uncertainty when picking fault cut-offs; c) Theoretical % error across a range of oblique transects for throw, heave, dip and displacement assuming a fault dip of 40˚. For throw, a throw gradient of 0.1 and a FW:HW displacement ratio of 1:4 was assumed. The shape of the theoretical % error graphs implies that heave, and therefore displacement and dip, will have a high theoretical error at high obliquity, whereas throw will have a lower theoretical error.

In this section we summarise the literature and theoretically expected contribution of each uncertainty element on the repeatability of fault data extraction.

Interpretation repeatability: The repeatability of measurements from seismic reflection data is influenced by human bias, leading to uncertainties in locating cut-offs (Schaaf and Bond, 2019). The position of cut-offs will be influenced by the interpreted horizon and fault, the interpreted intersection point and the projection of regional dip onto the fault plane. These factors are expanded upon below:

Interpreted horizons (Figure 1bi): Horizons picks are made along prominent reflections, ideally with consistent waveforms (Brown, 2011). Inconsistent waveforms can result in high rugosity structure maps, attributed to post-acquisition processing or geological features (Chellingsworth et al., 2015). Auto trackers and smoothing algorithms are commonly used to create geologically reasonable horizons, with the choice of methods used introducing subjective uncertainty (Brown, 2011; Chellingsworth et al., 2015). Previous studies have shown that horizon picking uncertainties decrease near wells, potentially due to an increase in interpreter confidence (Schaaf and Bond, 2019). Conversely, horizon picking uncertainties increase away from wells, especially in areas of low seismic image quality and near faults (Alcalde et al., 2017b; Schaaf and Bond, 2019). The image quality around faults can be affected by the presence of a damage zone, which can vary in width based on fault displacement and the structural position on the fault (Shipton and Cowie, 2003; Childs et al., 2009; Choi et al., 2016). Furthermore, correlating horizons across faults may be challenging due to variations in reflection properties, the presence of footwall degradation (Bilal et al., 2020), and/or changes in seismic stratigraphy in the footwall/hangingwall, and especially when reflectors cannot be traced around fault tips (Bond et al., 2007; Bond, 2015; Chellingsworth et al., 2015). We anticipate increased horizon picking uncertainty for faults with large displacement, at segment boundaries/fault tips, or in locations where footwall degradation has occurred.

Interpreted faults: Uncertainties in fault placement are influenced by the strength of seismic reflect and image quality (Alcalde et al., 2017b; Schaaf and Bond, 2019) (Figure 1bii). Interpretation uncertainty increases in areas with decreased reflector strength (Schaaf and Bond, 2019). Strong seismic reflectors overlying or underlying weak reflectors reduce uncertainty in our interpretation of the latter, and faults that conformed to expected geometries (e.g., matching the regional trend) are more reliably picked (Bond, 2015; Alcalde et al., 2017a; Schaaf and Bond, 2019).

Interpreted horizon-fault intersection (i.e., cut-offs): The way that reflections (mapped as horizons) intersect with faults, ie cut-offs, is open to interpretation and is therefore potentially uncertain. This arises at least partly from there being two components of fault-related deformation; *discontinuous*, which relates to the fault-related, brittle strain, and *continuous*, which relates to folding (i.e., ductile strain) and/or brittle deformation below the resolution of the seismic reflection dataset. As such, two types of fault cut-off are measured: discontinuous cut-offs, and continuous cut-offs (Figure 1b), which account for both the discontinuous and continuous components of deformation (Childs et al., 2017; Delogkos et al., 2017, 2020). These cut-offs can then be used to calculate fault throw, heave, dip, and displacement. The inclusion or not of continuous deformation depends on the scientific objective and the nature of the faulting. For example, to derive long-term fault slip-rates only the continuous portion of deformation is considered (Lathrop et al., 2021; Pan et al., 2021). In contrast, only the discontinuous portion is required to calculate lithological juxtapositions, shale gouge ratio and ultimately fault transmussivity.

Uncertainties affect cut-off types differently. Discontinuous cut-offs (Figure 1biii), are influenced by uncertainties in the position of the fault plane and horizon. Analysis of fault cut-offs suggests that areas of low image quality are associated with large uncertainty, leading to increased uncertainty with depth (Alcalde et al., 2017b; Schaaf and Bond, 2019). Moreover, cut-offs on faults with low displacement near the limit of separability (Magee et al., 2023) and the hanging wall cut-off of large displacement faults, which are deeper and due to additional accommodation space often show changes in seimic stratigraphy compared to the footwall (Alcalde et al., 2017b), are prone to higher uncertainties. Continuous cut-offs require the regional dip of the horizon to be projected onto the fault plane (Figure 1biv). In cases of small-displacement faults where continuous deformation comprises a significant portion of the displacement, the interpreter must choose where the fault intersects the deflected horizon (Faleide et al., 2021; Magee et al., 2023). This introduces uncertainty as there are multiple feasible locations for projecting the horizon onto the fault plane, and the position of the fault plane itself becomes more uncertain (Fig 1b). Where both types of deformation are present (e.g., fault growth through fault-propagation folding), the position of the fault plane will have lower uncertainty, but the interpreter still needs to subjectively determine where the regional dip transitions into near-fault continuous deformation.

Seismic image quality and the chosen vertical exaggeration are common factors that influence subjective uncertainties. To minimise their impact in our datasets, horizons at similar depths, with similar resolutions, are selected and a consistent vertical exaggeration is used during fault picking.

Previous studies have focused on the impact of subjective bias on data extracted from multiple interpreters (Bond et al., 2007, 2012; Bond, 2015; Schaaf and Bond, 2019). However, limited attention has been given to the consistency of an individual's interpretation. Magee et al. (2023) conducted a study where an individual made repeat picks on the same horizon of a low-displacement fault, revealing variations in fault cut-off positions that affected the extraction of throw and heave. Nevertheless, the datasets were found to be statistically equivalent and exhibited lower uncertainty compared to another interpreter's interpretation of the same horizon. Similar 'internal consistency' within individuals interpretations has also been observed in the field classification of faults and fractures (Andrews et al., 2019; Shipton et al., 2020) and seismic reflection-based models (Alcalde and Bond, 2022). This study aims to build on these findings by investigating the magnitude of individual internal consistency in fault properties, examining variations across different horizons, faults, cut-off types and measurement obliquity.

Measurement obliquity: Measurement obliquity is the angle relative to the fault strike that fault and fracture properties are sampled (Figure 1a), and it can affect the extraction of key properties such as spacing and dip (Terzaghi, 1965; Watkins et al., 2015). Optimal fault interpretation strategies for normal faults involves sampling using transects that are perpendicular to fault strike, i.e., parallel to the inferred slip vector, and avoiding measuring apparent dip. This approach reduces pick spacing along the fault, which is important for accurate interpretations of throw minima and fault segmentation (Michie et al., 2021).

Theoretical error estimates for the studied fault properties due to measurement obliquity can be obtained by considering the change in cut-off position caused by an oblique sample line (Fig 1c). For a fault with 40˚ dip, throw errors remain low even at high measurement obliquities (Fig 1ci). However, heave errors exceed 50% at measurement obliquities of ±50˚ and exceed 10% at a measurement obliquity of ~25˚. These errors would lead to moderate over- and under-estimates of displacement and dip, respectively, at high measurement obliquities. Therefore, we expect measurement obliquity to have a small effect on the extraction of throw, but greatly impact measurements of heave, and therefore displacement and dip (Fig 1c).

Given the non-linear morphology of faults and the scale-dependant nature of strike, ensuring all data are extracted using orthogonal transects can be difficult and time intensive. Furthermore, if 2D seismic lines are the only available datasets, the lines may not be optimally orientated (i.e., perpendicular) to local fault strike. This study aims to investigate the threshold at which measurement obliquity significantly affects the extraction and interpretation of fault properties, and therefore to provide quantified errors that can be applied to other studies.

2. Dataset/methodology

2.1 Seismic data

We use a high-resolution 3D seismic survey (Chandon3D) located on the Exmouth Plateau, offshore NW Australia (Fig 2). Chandon3D is a time-migrated, zero-phase survey that has a record length of 6 seconds two-way time (TWT) and bin-spacing of 25 m. The data are displayed with a SEG reverse polarity, i.e., a downward increase in acoustic impedance corresponds to a trough (black) reflection, and a downward decrease in acoustic impedance corresponds to a peak (red) reflection (Figure 1b). We used four wells to constrain the age and lithology of mapped reflections (Chandon-1, Chandon-2, Chandon-3, Yellowstone). Check shot data from these boreholes were used to establish the time-depth relationships for the seismic survey, which we use to convert measurements in TWT to meters (Supplementary 2). Using this time-depth relationship and given the dominant frequencies in the interval of interest are ~30-40 Hz, the limits of separability and visibility are estimated at ~20±4 m and 3±1 m respectively (Magee and Jackson, 2020a). Where reflectors are separated by a distance below the limit of separability, individual reflectors cannot be resolved and they will appear as a tuned reflection package (Brown, 2011) (i.e., no discontinuous deformation will be visible). This resolution is sufficient to enable the investigation of small errors in our datasets caused by the three elements of interpretation uncertainty we are interested in.

2.2 Geological setting

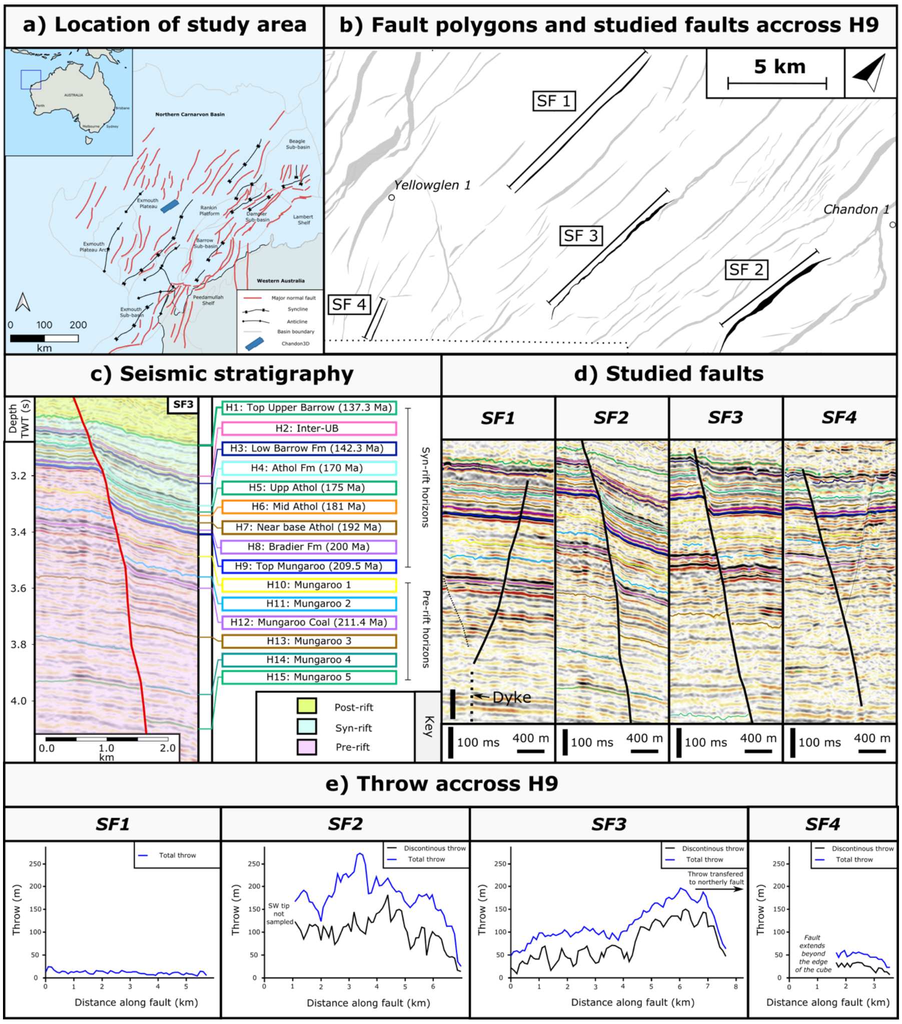

Figure 2: Regional geology and studied faults: a) Overview of the North Carnarvon Basin showing the major faults and sub-basins (adapted from Bilal and MacClay, 2021). The study area, as marked as a blue box, is not located on one of the major faults and as such displays little footwall degradation compared to other faults in the area; b) fault polygons for Horizon H9, highlighting the location of the four quasi-straight faults studied; c) Seismic stratigraphy highlighting the key horizons used in this study; d) strike-perpendicular transects for each fault showing the structural style of each fault; e) along-strike profiles depicting the thow extracted using discontinuous (black) and continuous (i.e., total throw) (blue) cut-offs across the H9 horizons for data extracted using an strike-perpendicular transect. Note that the difference between the two lines represents the magnitude of deformation accommodated by folding and/or sub-seismic scale faulting.

The study area is situated in the Exmouth Plateau region of the Northern Carnarvon Basin, offshore NW Australia (Figure 2a). The region experienced several phases of rifting from the Late Carboniferous to the Early Cretaceous (Tindale et al., 1998; Stagg et al., 2004; Direen et al., 2008). The Triassic to recent tectono-stratigraphy of the Exmouth Plateau can be divided into four main megasequences (Bilal and McClay, 2022). The main phase of WNW-directed extension, which is associated with deposition of Megasequence-II, resulted in the formation of north-south striking normal faults, including three of the four faults we focus on (SF1, 3, 4) (Figure 2b) (Stagg et al., 2004; Bilal et al., 2020; Bilal and McClay, 2022). During rifting, the basin was sediment-starved, meaning it now contains a relatively condensed (≲100 m thick), largely marine syn-rift succession (Karner and Driscoll, 1999). This succession is separated from the overlying Late Jurassic marine Dingo Claystone by the end-Callovian regional unconformity (Tindale et al., 1998; Yang and Elders, 2016; Bilal et al., 2020; Bilal and McClay, 2022). Tectonic faulting slowed, or stopped, during the Late Jurassic, but resumed after the formation of the regional unconformity (~148 Ma), being synchronous with the deposition of the Barrow Group (~148 to 138 Ma) (Gartrell et al., 2016; Reeve et al., 2016; Paumard et al., 2018). During the second phase of faulting, new N-S to NW-SW striking, low-throw (<0.1 km) normal faults developed (Black et al., 2017), with some of the earlier faults being reactivated (Bilal and McClay, 2022). Continental breakup occurred during the Early Cretaceous (~135 to 130 Ma) was followed by thermal subsidence and passive margin development (Robb et al., 2005; Direen et al., 2008; Reeve et al., 2021).

In addition to tectonic faults, a series of dyke-induced faults are identified across the study area (Magee and Jackson, 2020b, 2020a; Magee et al., 2023), of which SF2 is an example. These dykes are expressed as sub-vertical, low-amplitude zones that disrupt the seismic reflectors within the pre-rift sedimentary succession (Magee and Jackson, 2020b). Several associated grabens occur directly above and along the dykes, bound by oppositely dipping faults that intersect with the upper dyke-tip (Magee and Jackson, 2020b, 2020a). These dyke-induced faults are often long (10s km), show variable dip and displacement distributions along strike, typically have low maximum throw values (often <50 m), and terminate upwards at the Base Cretaceous unconformity (Magee and Jackson, 2020b, 2020a; Magee et al., 2023).

Four sub-linear faults (SF1-4) were analysed in this study, varying in length from 2.4 to 7.9 km and exhibiting maximum total throw (i.e., throw extracted using continuous cut-offs) ranging from 32 to 273 m (Fig 2b, d, e). Discontinuous and continuous cut-offs can be measured for faults SF2-4; however, the average throw across SF1 (13 ± 6 m) is between the limit of separability and visibility for the seismic cube. Therefore, only a small number of picks along this fault display discontinuous throw, meaning we report only data extracted from continuous cut-offs for this fault. Figure 2e shows the throw distributions of the base syn-rift horizon (H9), showing variations between faults. Along Horizon 9, faults exhibit moderate dips (52˚ ± 8˚) with lower dips observed at shallower depth, within the syn-rift succession (H1 = 32˚ ± 6˚).

The studied faults have been buried beneath a thick layer of post-Cretaceous sediments, which can lead to compaction and rotation of pre-existing structures to shallower dips (Allen and Allen, 2013). Burial-related compaction will also act to reduce the throw across syn-sedimentary faults by <15% in sand-shale mixed lithologies (Taylor et al., 2008) similar to those observed in the study area (Bilal and McClay, 2022). However, decompaction was not performed in this study due to uncertainties in decompaction parameters, particularly for more deeply buried hanging wall sediments not sampled by well data. As a result, the extracted values of fault throw, dip and displacement represent minimum estimates. Since all faults have been buried to a similar depth, the impact of compaction on the extracted fault properties should be consistent across the datasets, and thus should not affect our statistical analysis or related conclusions.

2.3 Sample strategy

Oblique transects relative to fault strike were created close to the location of maximum throw at an interval of 10˚ from perpendicular to the quasi-striaght fault. This resulted in a total of 11 transects for each fault (i.e., from 0˚ to ±50; Fig 1a). Each transect was then transposed to parallel positions 100 m apart using the arbitrary line tool in DUGInsight to enable sampling (following the strategy shown in Fig 1a). This means that for oblique datasets, the along-strike distance between adjacent cut-offs will be > 100 m (~156 m for 50˚ obliquity) and the exact location on the fault the data is collected from will differ between transects of different obliquity.

At each sample location, we collected discontinuous and continuous cut-off data for 8-13 horizons, depending on the regional continuity of mapped reflectors. For the discontinuous cut-offs, we identified the location where the horizon intersects the fault in the footwall and hanging wall (Fig. 1a). In cases where continuous deformation was present, we projected the regional horizon dip onto the fault plane and measured the intersections in the hanging wall and footwall (Fig. 1a). Depth values were converted from two-way travel time (TWT) to metres, and the following fault properties were calculated: throw, heave, dip, and displacement (Fig. 1a). For dip and displacement, we assumed that the slip vector is dip-parallel (cf. Magee and Jackson, 2020a). Where both discontinuous and continuous cut-offs are extracted (along SF2-4), we also calculated the ratio between the different types of throw.

To facilitate the plotting and comparison of data between oblique and strike-perpendicular transects, we determine the equivalent sample location of the cut-offs relative to the strike-perpendicular transect. This allows us to calculate the distance along the fault that the data is collected from. For oblique cut-offs, the equivalent strike-perpendicular sample location will differ for the footwall and hanging wall (Fig 1a). To account for this, we take an average of the two cut-offs to obtain the equivalent strike-perpendicular sample location.

2.4 Data presentation and statistical analysis

We analyse and present our data on three aspects of fault interpretation uncertainty: interpretated measurement type, interpretation repeatability, and measurement obliquity. We examine these aspects using dataset statistics and individual picks. Dataset statistics involve statistically comparing population means or medians to determine ther equivalence, with our approach outlined in Supplementary 8. To compare datasets based on specific uncertainty element (e.g., obliquity, cut-off type), we report the average difference between population means, the average percentage (%) difference, and the proportion of datasets that can be considered equivalent. Aggregated dataset statistics allow for a direct comparison of properties with varying dataset numbers (e.g., different faults). Initially, we combine and discuss the obliquity and repeatability statistics for each fault property (i.e., take the average values for absolute difference, % difference, and % of equal datasets of the discontinuous and continuous datasets). Subsequently, we compare discontinuous and continuous obliquity and repeatability datasets in the same manner as described above and in Supplementary 8.

3. Results and the impact of uncertainties on fault properties

In this section we initially discuss the effect of our three investigated uncertainty elements (i.e., interpretation repeatability, measurement obliquity, and measurement choice) for combined extracted fault properties (Section 3.1), before considering their impact on individual properties (i.e., throw, heave, displacement, dip) (Sections 3.2 to 3.4).

3.1 All fault properties

Repeatability: Among all repeatability datasets, only 46% (283 out of 616) were statistically equivalent, with an average difference in population mean/median of 16% (Table S1). The percentage of equivalent datasets varied between faults, ranging from 31% (SF1) to 56% (SF2), and the difference in population means ranged from 9% (SF2) to 28% (SF1). Repeat picks showed more uncertainty for H9 (32% equivalent datasets, 20% difference) compared to H12 (59% equivalent datasets, 13% difference). This trend was consistent across all faults, although the magnitude of difference caused by horizons varied between faults. Overall, less than half repeat datasets could be considered equivalent, and the percentage difference depended on the fault and horizon from which the data was extracted.

Obliquity	a) % of oblique datasets that are statistically equal to the fault perpendicular dataset					Colour scale	b) % error between oblique and fault perpendicular datasets					Colour scale
	SF1	SF2	SF3	SF4	All faults		SF1	SF2	SF3	SF4	All faults	
-50	20%	28%	29%	54%	34%	Maximum value	65%	28%	38%	35%	38%	Minimum value
-40	45%	19%	38%	64%	40%		26%	26%	26%	22%	25%	
-30	61%	38%	45%	83%	54%		17%	15%	17%	15%	16%	
-20	73%	72%	74%	88%	77%		13%	10%	8%	12%	10%	
-10	80%	84%	91%	95%	89%		16%	6%	4%	9%	7%	
10	73%	58%	66%	86%	70%	Median	13%	10%	10%	11%	11%	Median
20	61%	88%	56%	85%	73%		19%	6%	12%	14%	12%	
30	39%	38%	42%	88%	52%		5%	15%	16%	18%	19%	
40	57%	30%	31%	58%	41%		21%	22%	25%	29%	25%	
50	30%	23%	22%	64%	34%		43%	41%	42%	25%	38%	
Total	**54%**	**48%**	**49%**	**76%**	**56%**	Minimum value	**27%**	**18%**	**20%**	**19%**	**20%**	Maximum value

Figure 3: The effect of obliquity on extracted fault properties: a) the percentage error of all fault properties split by fault and obliquity; b) the % of datasets for that fault and obliquity that are statistically equal to the dataset extracted for that horizon using an strike-perpendicular transect. Colour scales differ between individual faults and all fault datasets so that red represents datasets that are highly affected by obliquity, and blue represents datasets where obliquity has a limited effect on extracted fault properties. Note how most values are blue (smaller errors) where obliquity is <± 20˚, suggesting that oblique sampling above this value should be avoided to minimise obliquity related errors.

Obliquity: Greater errors were observed where the degrees of obliquity exceeded 20˚ (Fig. 3). The same overall pattern was observed for individual faults, although there was more scatter in the data (Fig. 3). The percentage difference for any given obliquity also varied for each fault. Some horizons are more prone to obliquity related errors (Table S2), suggesting that horizon properties (e.g., reflection amplitude) contribute to interpretation errors. Nevertheless, all horizons exhibited the same general trend of increased uncertainty with increasing obliquity.

Interpreted cut-off type: The effect of cut-off type differed between obliquity and repeatability datasets. For repeat interpretations, little difference was observed in the uncertainty between continuous and discontinuous cut-offs, with 48% and 44% of datasets considered equal. Conversley, the obliquity datasets displayed greater uncertainty for continuous cut-offs (51% equal datasets) when compared to discontinuous cut-offs (63% equal datasets) (Table 2). The horizon where the cut-offs were measured influenced the error and uncertainty of the extracted data. Some horizons exhibited low or high percentage differences and proportion of equal datasets for both measurement types (e.g., Horizons 9 and 10). However, certain horizons showed greater uncertainty in data extracted from continuous cut-offs (e.g., H13 and H14) (Table S2). This suggests the interpreted cut-off type has a moderate effect on obliquity datasets and a minor to negligible effect on repeat picks, with the horizon from which the data is extracted being a key controlling factor on the magnitude of uncertainty.

Overall, when considering all fault properties, the interpreted cut-off type, the magnitude of obliquity, and the fault and horizon from which the data is extracted, are identified as key factors controlling interpretational uncertainty. To assess the effect of obliquity on repeatability, it is important to separately considered the influence of uncertainty factors on each fault property separately. This approach allows for the isolation of factors and the comparison of obliquity errors to the theoretical errors introduced in Figure 1c.

3.2 Throw

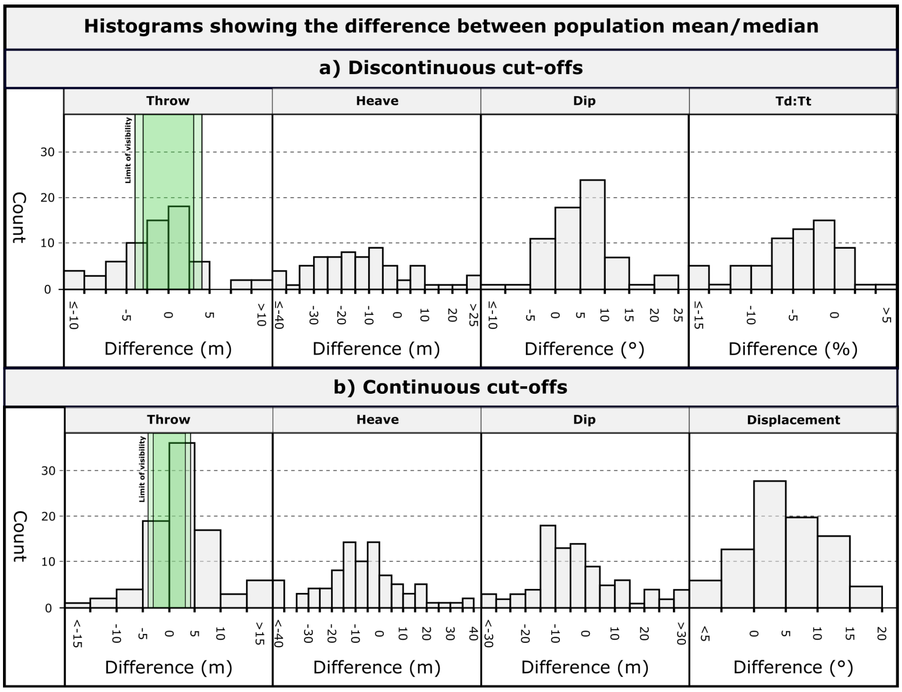

Figure 4: Histograms to summarise the mean/median difference in fault properties extracted from discontinuous (a) and continuous (b) cut-offs between repeat picks at identical points, across a series of horizons and faults. Each 'count' represents a population mean or median for all data points collected for a single horizon across a single fault. The green box on the throw histograms highlights the minimum and maximum limit of visibility for the seismic cube. Differences within this box can be considered as below the resolution limit, and therefore not caused by repeatability errors. Note that for all extracted properties, continuous measurements show lower repeatability than discontinuous measurements.

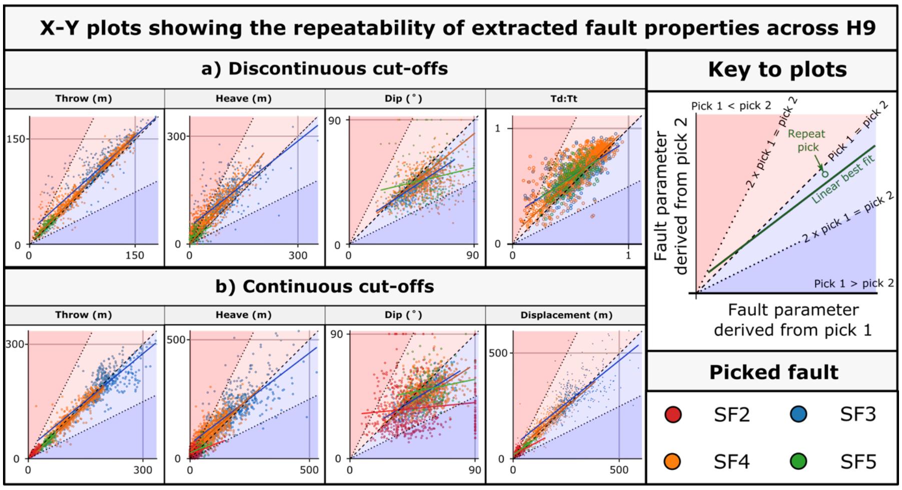

Figure 5: x-y plots showing the variations in repeatability in discontinuous (a) and continuous (b) fault properties extracted from horizon H9 across all faults. If the interpretation is repeatable, then all points should plot along the black dashed x-y line; however, where picks differ the points will plot within the red or blue zone depending on the ratio of pick values. Data plotting in the darker red or blue zones represent data where one pick is over double the other. Note how the difference between picks varies between faults, extracted property, and the magnitude of the extracted property. Additionally, throw shows less repeatability error than heave.

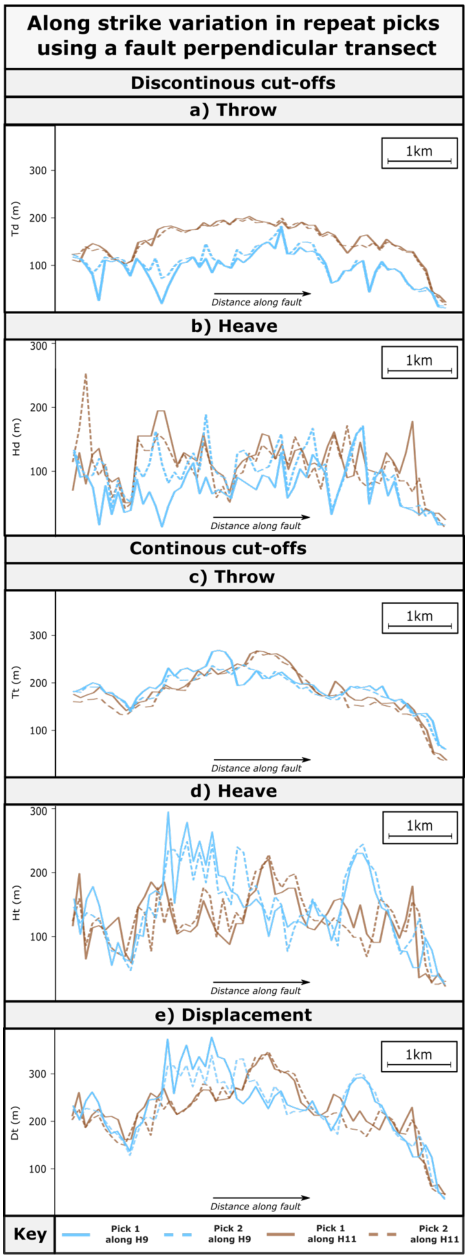

Figure 6: Along-strike profiles showing the repeatability of fault property extracted from H9 and H12 using a strike-perpendicular transect along SF2. Pick one is shown as a solid line, whilst pick two is dashed and each horizon is a different colour. Note how the general shape of the profiles are similar between picks; however, the difference can be locally quite large.

Repeatability: Throw exhibits low uncertainty across all repeatability datasets (Table S1, Fig 4, 5), with 60% of datasets considered equivalent, and there being only small differences in means (5m, 7.4%). The mean absolute difference differs between faults, with differences across all faults typically below the estimated seperability limit of the seismic data (Table S1). Whereas differences in population means are minimal, this was not the case for all picks along the fault. For example, Figure 6a and 6c shows multiple locations where the difference between picks on throw profiles extracted from discontinuous and continuous cut-offs exceeds 22 m. The profiles also highlight sections of the fault with high and low differences between picks, and that the location of these sections are not consistent between horizons (i.e., H9 may show high variability at a particular along-strike location where H12 shows low variability, and vice versa). This suggests that whereas horizons have a limited effect on population statistics, they do influence individual picks. Overall, repeatability errors primarily affect throw at a local scale (e.g., <500 m) and have a negligible effect on population statistics.

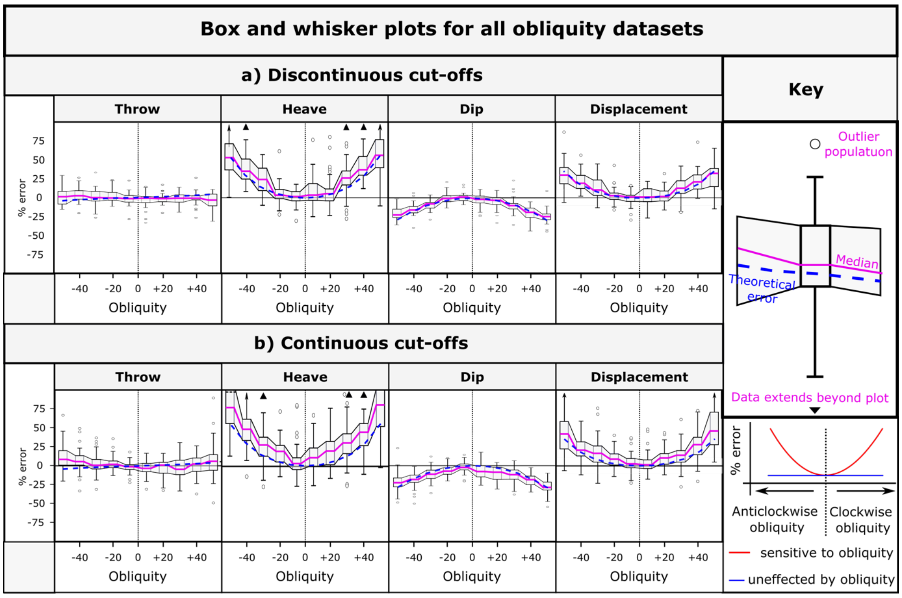

Figure 7: The effect of obliquity on individual fault properties extracted from discontinuous (a) and continuous (b) cut-offs. Box and whisker plots are constructed from the population mean/medians of individual horizons picked across individual faults. Note how obliquity has the greatest effect on heave, and therefore dip and displacement, suggesting that additional care needs to be taken when sampling fault cut-offs for these properties. Furthermore, the median % error for all datasets typically exceeds the theoretical value for continuous cut-offs, suggesting some of the error is caused by non-geometrical effects.

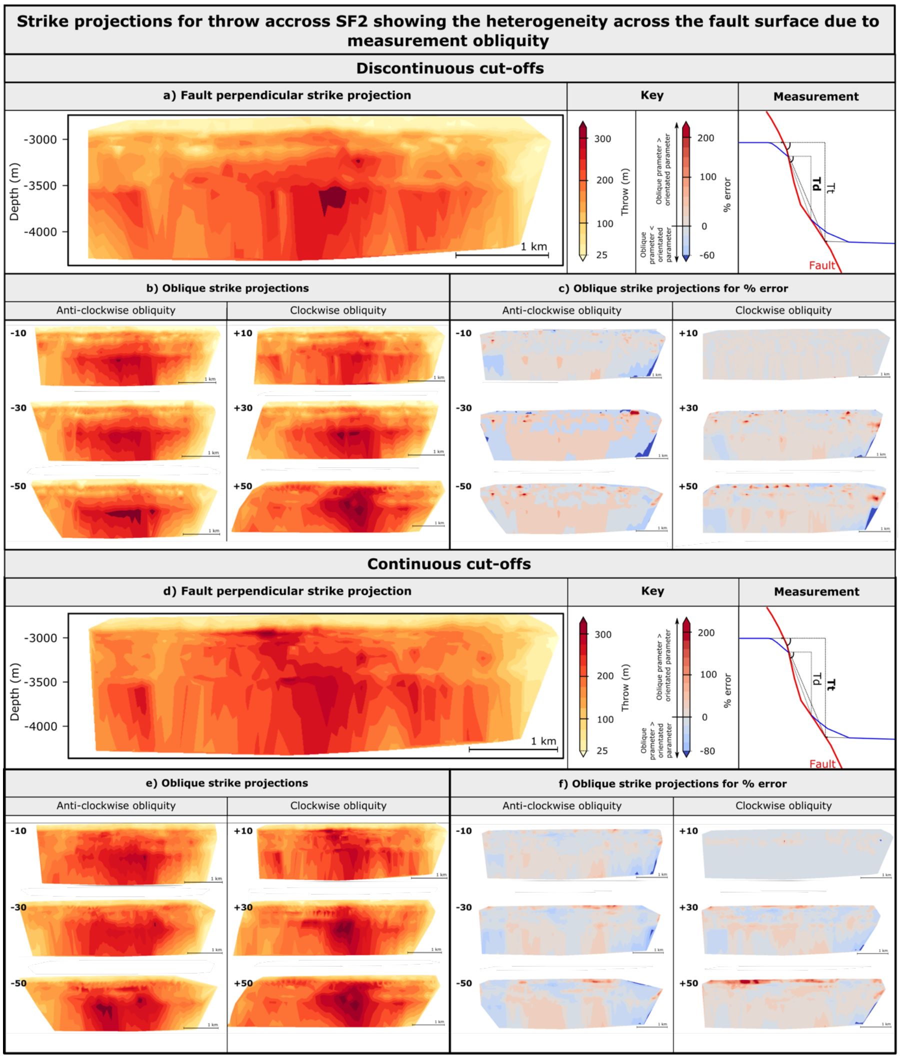

Figure 8: Strike projections showing the along-strike and down-dip variability caused by oblique sampling for throw extracted using discontinuous (a-c) and continuous (d-f) cut-offs along SF2. Data extracted from strike-perpendicular (a & d) and oblique (b & e) transects are shown, along with the % error associated with the oblique measurement (c & f). Note how the distribution and % error of throw depends on both the direction and magnitude of measurement obliquity. Strike projections are created using a python script that undertakes a linear interpretation between known datapoints, resampled to a regular sample spacing to enable the % difference between datasets to be calculated.

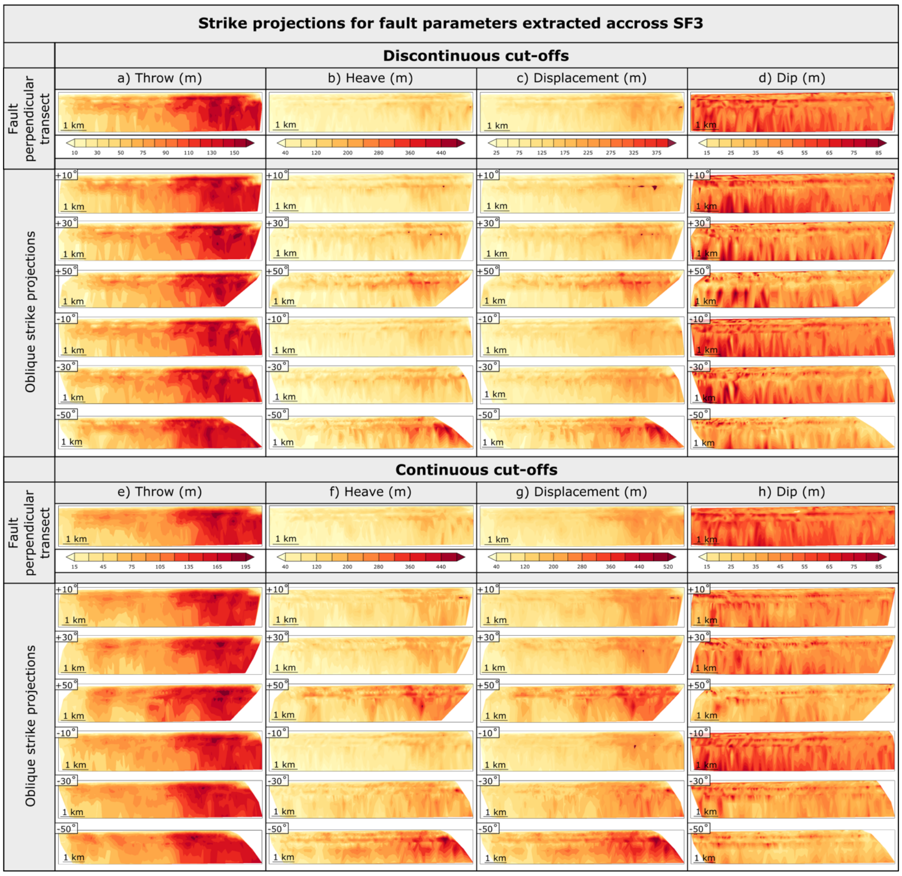

Figure 9: Strike projections showing the along strike and down dip vraibily of all studied fault properties calculated from discontinuous (a-d) and continuous (e-h) cut-off data extracted from SF3. Note how throw is less sensitive to measurement obliqutity than heave and displacement and that dip shows high spatial variability across all datasets.

Obliquity: Overall, throw typically displays increasing uncertainty as the obliquity increases (Table S2, Fig. 7); however, the error across the range of obliquity is low. Where individual faults are considered, not all faults show greatest error at high degrees of obliquity (e.g., SF1, SF4; Table S3). The picked horizon also has a large impact on the % difference for throw, although the overall trends of increasing uncertainty with increasing angles of obliquity are still observed. The distribution of throw across the fault plane varies at different degrees of obliquity (Figure 8, 9a, 9e) and can be over- or under- estimated at different locations, with % errors locally exceeding 100%. Overall, our data suggests that horizon properties (e.g., acoustic impedence, amplitude of the reflection) strongly affect the measurement of throw and the effect of measurement obliquity depends on the fault the data is extracted from. Obliquity errors exceed the theoretical geometrical errors (Figure 1c) for throw for faults by <±5%, with some horizons exceeding the expected error by a factor of 5 (Figure 7). The repeatability of throw does not appear to be sensitive to the degrees of obliquity as highlighted by: i) the distribution of statistically equal datasets and ii) given angle of obliquity can show both high and low % differences for the same cut-off type and horizon (Figure 10).

Interpreted cut-off type: The interpreted cut-off type affects the magnitude of repeatability and obliquity errors. Average repeatability errors for throw are marginally higher for continuous cut-offs (6.0 m, 9%) compared to discontinuous cut-offs (4.0 m, 5%) (Table S1). In most cases, H9 showed greater errors compared to H12 for both cut-off types, with the only exception being continuous cut-offs extracted from SF2 (Table S1). The magnitude and location of along-strike variations between individual picks differed between horizons and cut-off type (Fig 6). Indeed, there are examples where throw calculated from the first discontinuous cut-off pick exceeds the second, with the opposite being true for continuous cut-offs. For oblique transects, a far greater proportion of datasets are equal (91%), with a lower % error (7%) for discontinuous cut-offs when compared to continuous cut-offs (75%, 11%; Table S7, S8). The magnitude of error increases for low-throw faults where t the same horizons show large and small error, albeit with continuous cut-offs showing a greater errors. The distribution of throw along- and down- dip is highly variable at different degrees of obliquity (Fig 8, 9a, 9e), with the distribution and magnitude of throw depending on the direction and degrees of obliquity. Additionally, the patterns are not constant between discontinuous and continuous cut-offs, as shown by the location of throw maxima in Figure 8b and e.

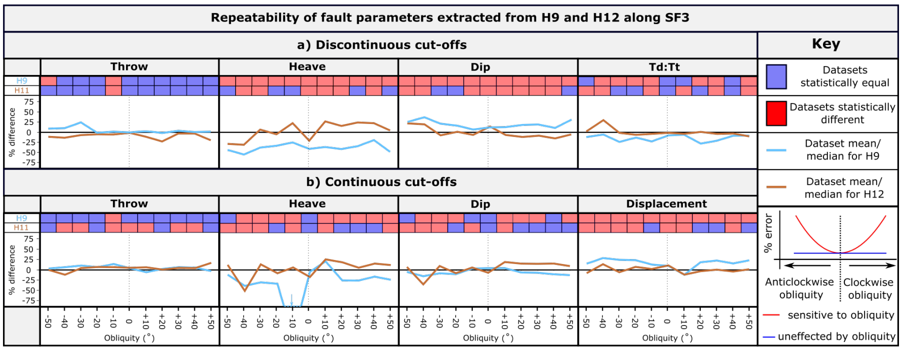

Figure 10: Repeatability of fault picks for fault parameters extracted using discontinuous (a) and continuous (b) cut-offs along horizons H9 and H12 for SF3. The plots show whether pick one and pick two can be considered equal, and the mean % difference between each pick. Note how there is no correlation between obliquity and repeatability error, suggesting that obliquity and repeatability are independent sources of error for this dataset.

3.2 Heave

Repeatability: Heave shows high uncertainty across all repeat picks (Fig. 4, 5), with only 37% of datasets considered equivalent and a reasonable difference between population mean/median values (17.8 m, 27%). SF2 is less prone to repeatability errors when compared to other faults (Fig. 5; Table S1). Repeatability errors are greater at lower values of heave, as indicated by the higher % difference for SF1 and the x-y plots in Figure 5. Along-fault heave profiles (Fig. 6b, d) show a large variability in the magnitude and difference between picks for adjacent measurement positions (i.e., a large amount of noise in the data). Errors are not consistent between horizons or measurement types and the difference between picks can locally exceed 50 m (Fig 6b, d). This suggests that repeatability errors in fault and horizon picks and how these vary along-strike effect the extraction of heave, creating uncertainty in heave measurements.

Obliquity: The degree of obliquity has a large effect on heave, with uncertainty increasing with increasing degrees of obliquity (Table S4). The mean absolute difference in heave exceeds the average difference for repeat picks at obliquities of ±30˚ and shows a maximum difference of 54.3 m (72%). This trend is observed across all faults; however, each fault shows a different magnitude of error and proportion of equal datasets, with SF2 and SF3 appearing to be most prone to obliquity errors. When compared to theoretical geometric errors (Figure 1c, 7) most datasets show % errors that exceed the expected values by between 5% and 10%, with the heave measurement for some horizons being particularly prone to high errors. The effect of obliquity on the distribution of heave across the fault plane depends on the fault and the direction and degree of obliquity (Figure 9b, f). For all faults, the overall trend is that as obliquity increases, the proportion of positive % difference also increases (irrespective of the absolute magnitude of heave). On top of these general trends however there is a large amount of scatter which for some faults (e.g., SF1) lead to a high spatial variability in heave (Figure 9b, f). For all datasets, the angle and direction of obliquity does not appear to affect the % difference between picks (Fig 10). Overall, the degree of obliquity greatly affects the measurement of heave, with the error compounded by large differences between along-strike sample locations.

Interpreted cut-off type: The interpreted cut-off type has a large effect on obliquity statistics, although the effect on repeatability depends on the fault which the data are extracted from (Table S1, Figure 10). For repeat picks, heave extracted from continuous cut-offs shows a smaller difference in population mean (16.5m, 26%) and a higher proportion of equivalent datasets (41%) compared to discontinuous cut-offs (19.0 m, 33% and 28% respectively). However, this is not the case for SF2 where the opposite is true. Both cut-off types show large along-strike variability; however, continuous cut-offs show less differences between adjacent sample locations then discontinuous cut-offs (Figure 6). The measurement of continuous cut-offs greatly increase the % error in obliquity statistics, with the error nearly always greater than discontinuous cut-off data and the theoretical geometrical error (Figure 1c, 7). Smoother profiles observed in the repeatability datasets are mirrored where heave is calculated from continuous cut-offs, with these strike projections appearing less noisy than the discontinuous cut-offs (Figure 9b, f).

3.3 Displacement

Repeatability: Displacement shows moderate uncertainty across all repeat picks (Table S1, Figures 4, 5) with 47% of datasets considered equivalent and an absolute difference of 15.3

m (16%). The level of uncertainty differed between faults, with SF1 displaying the lowest number of equivalent datasets (27%) and greatest % error (31%). The along-strike displacement profiles (Figure 6e) show the same along-strike variability observed in the heave profile, but with a lower magnitude of variability caused by the low variation in throw. Sections of faults that show high, or low, differences between picks are more laterally extensive (up to 1.5 km) than heave and match more closely the differences observed in throw (Figure 6e).

Obliquity: Displacement exhibits increasing uncertainty at higher degrees of obliquity, surpassing repeatability errors at ±30˚ (Table S5). The pattern observed in heave strongly impacts the population statistics, with SF2 and SF3 showing the lowest proportion of consistent datasets. Displacement varies across fault planes, with increasing magnitude at higher obliquities (Figures 7, 9c, g). Like the heave datasets, the base syn-rift displays a pronounced displacement maxima and significant variability between along-strike data points (Figure 9c, g). Measurement obliquity does not systematically effect the repeatability of fault displacement (Figure 10). Overall, displacement is more susceptible to the degree of obliquity than throw, with uncertainty in heave influencing the magnitude of displacement and how this varies along the length of the fault.

Interpreted cut-off type: Interpreted cut-off type impacts repeatability and obliquity errors differently (Table S1, Figure 7, 10). Displacement calculated from discontinuous cut-offs exhibits greater differences between picks, and a lower proportion of equivalent datasets compared to continuous cut-offs (Table S1). Both cut-off types show increasing uncertainty with increasing degrees of obliquity; however, the magnitude of difference is greatest for continuous cut-offs (Figure 7). However, for some faults, highly oblique continuous cut-off datasets may exhibit low uncertainty (e.g., SF4, Table S12) and the displacement strike projections constructed for continuous cut-offs are smoother than discontinuous cut-offs (Figure 9c, g). Despite this, repeatability errors are usually exceeded where measurement obliquity is at or above ±30˚. Overall, interpreting continuous cut-offs reduces the repeatability of displacement on some horizons and measurement obliquity greatly affects continuous datasets .

3.4 Dip

Repeatability: Of all the fault properties, dip exhibits the highest uncertainty in repeat picks (Figure 4, 5, Table S1), with only 32% of datasets considered equivalent and an absolute difference of 6.6˚ (16%). The fault from which the data is extracted from influences the magnitude of uncertainty in dip, with SF1 showing a mean absolute difference of 9.2˚, whereas SF2 only has a difference of 3.2˚. Unlike heave and displacement, the magnitude of dip appears to only have a weak effect on repeatability (Figure 5). Individual picks on SF1 show very large differences, with several picks having a dip of 90˚ (indicating zero heave), whereas the paired pick ranges from ~15˚ to ~65˚ (Fig 5). These picks are taken from where there are very small offsets along SF1, thus heave is likely below the resolution the data is extracted (minimum heave values of ~6 m). Due to the compound errors caused by the uncertainty in heave, dip shows low repeatability and along-strike variations can be masked by measurement errors (Figure 9d, h).

Obliquity: Fault dip is strongly affected by measurement obliquity, with repeatability errors exceeded for most oblique datasets (Figure 7, Tables S1, S5). In a similar manner to displacement, the effect of uncertainties on heave strongly affects the calculation of dip (i.e., SF2 and SF3 showing the lowest % of equal datasets), although greater uncertainty is observed for the latter (Table S5). Repeatability errors are exceeded where the angle of obliquity exceeds ±20˚ for all faults, apart from SF1 where repeatability errors were particularly high (Table S5). The distribution of dip across the fault plane displays a high degree of variability between points leading to noisy strike-projections (Figure 9d, h). Despite this, general trends are observed across all obliquities (e.g., shallower dips at the syn-rift horizon (H9)); however, the magnitude of dip is lower at higher degrees of obliquity. In most cases, there is no correlation between the degree of obliquity and repeatability (Figure 10).

Interpreted cut-off type: The choice of cut-off type affects repeatability and obliquity datasets differently. Across all faults, the choice of cut-off type does not affect the repeatability of dip, with similar differences and percentage of equal datasets observed. Whether discontinuous or continuous cut-offs show greater uncertainty depends on the fault and horizon the data is collected from, with H9 broadly showing greater uncertainty than H12. Where individual picks are considered, there is more scatter where continuous cut-offs are measured (Figure 5), with many picks exceeding 100% difference. Despite this, profiles constructed from continuous cut-offs show less along-strike variability (Figure 5). Measurement obliquity affects both cut-off types; however, the effect is greater where continuous cut-offs are measured (Table S13, S14). This trend is observed across all faults, however, the magnitude of error and difference between cut-off types depends on the fault and the horizon that the data are extracted from. It is difficult to assess the effect of cut-off type on the distribution of dip across the fault plane as both exhibit a highly variable distribution of dip across the fault plane for all datasets (Figure 9d, h). Overall, no systematic difference between cut-off type is observed for the the repeatability of dip and whereas the measurement of continuous cut-offs increases errors associated with obliquity, datasets are very noisy and it is not possible to deduce along-fault trends.

3.5 Summary of results

Our data show that fault properties extracted from fault-horizon cut-offs are variably influenced by interpretation repeatability, measurement obliquity, and the measured cut-off type (Table 1). When all properties were considered together, less than half of the datasets could be considered statistically equal. Errors due to measurement obliquity were found to greatly increase when obliquity exceeded ±20˚. Measurements of continuous cut-offs showed greater errors than discontinuous cut-offs in both the obliquity and repeatability datasets. The magnitude of error was also influenced by which fault and horizon the data were collected from.

When individual fault properties are considered, throw is found to be the least sensitive fault property to the studied interpretation factors, and heave the most sensitive (Table 1). The uncertainties in throw increased when measurement obliquity exceeded ±20˚; however, the magnitude of uncertainty was often below or close to the limit of separability of the seismic cube (i.e., not a significant source of error) apart from at a local (<500 m) scale. Heave was found to show statistically significant differences for both repeat and oblique datasets. Differences were particularly evident at a local scale and caused strike projections and along-strike profiles to be noisy. The fault and horizon cut-off data were extracted from had a subsidiary effect on extracted fault properties (e.g., heave and throw) and the magnitude of obliquity did not appear to compound repeatability errors for any fault property. Across most fault properties, continuous cut-off picks were more susceptible to repeatability and obliquity errors. Despite showing greater uncertainty for continuous picks, continuous datasets show less along-strike variability between adjacent picks, leading to smoother along-fault profiles and strike projections. The ratio of throw extracted from discontinuous to continuous cut-offs indicates that the errors from the continuous and discontinuous datasets were compounded where the properties were compared, and the noisiness of the discontinuous profiles lead to large variations in the ratio between discontinuous and continuous throw between adjacent picks across a fault. Uncertainty in heave also increases uncertainty in displacement and dip (as these properties are geometrically derived using heave), with the effect particularly noticeable in a long-fault profiles and strike projections. For dip, it was found that this local scale uncertainty often masked overall trends in dip and caused profiles and strike projections to be very noisy (Figure 9d, h). In the following section, we investigate how the aforementioned uncertinaies in cut-off derived fault properties affect the assessment of fault transmusivity and the evolution of throw- and slip-rate through time.

Fault property	Repeatability	Measurement obliquity	Interpreted cut-off type
All fault properties	Repeat datasets are often not equivalent, with the % difference depending on the fault and horizon that the data is extracted from.	Error is found to increase where obliquity exceeds ±20˚. The fault and horizon that the data is collected from also has a subsidiary effect.	Greater uncertainty in continuous cut-offs compared to discontinuous; however, the difference is low to moderate for obliquity datasets and negligible for repeat picks.
Throw	High repeatability Errors only significant at a local scale (i.e., <500 m).	Moderate sensitivity Errors increase as obliquity increases and are larger than predicted. Overall differences in population means are generally small.	High sensitivity Uncertainty increases in faults with low throw. Throw distribution is variable and influenced by the horizon and measurement obliquity.
Heave	Low repeatability Depends on the fault, horizon, and along-strike position that the data is collected form.	High sensitivity Errors are compounded due to differences between along-strike sample locations.	High sensitivity Continuous cut-off data exhibits smoother along-strike profiles but with increased errors at high obliquities.
Displacement	Moderate repeatability Along-strike patches of low repeatability more closely	High sensitivity	Moderate sensitivity

	match the shape of the throw profile.	Due to high uncertainty in heave influencing the distribution and magnitude of displacement.	Measurement obliquity greatly effects continuous cut-off datasets, whilst also causing strike projections to be smooth.
Dip	Low repeatability Along-strike variations are often obscured by measurement errors	High sensitivity Overall dip increases with obliquity, and there are large spatial variations across the fault plane.	Low sensitivity Datasets are very noisy and it is not possible to deduce along-fault trends.

Table 1: Summary of the effects of interpretation uncertainty on the extracted fault properties. Note how heave is more prone to interpretational uncertainty than throw, which also affects the extracted dip and displacement.

4 Effect of obliquity and repeatability uncertainty on inferred fault properties

Data extracted from 3D seismic reflection surveys are used across a range of scientific studies, and therefore the sources of uncertainty presented in this paper have implications for the geological interpretations that arise. Drawing on data from SF2, w discuss the implications for two such interpretations, fault transmissivity which is important for quantifying fluid flow, and slip/throw rates used to inform seismic hazard assessment. Throw extracted from discontinuous cut-offs is used for fault transmissivity and throw-rate calculations, whereas continuous cut-offs are used when assessing the evolution of slip-rate to account for non-descrete deformation (e.g., monocline development). These examples demonstrate the practical effect of the investigated uncertainty elements on fault property predictions.

4.1 Fault transmissivity interpretation using discontinuous deformation

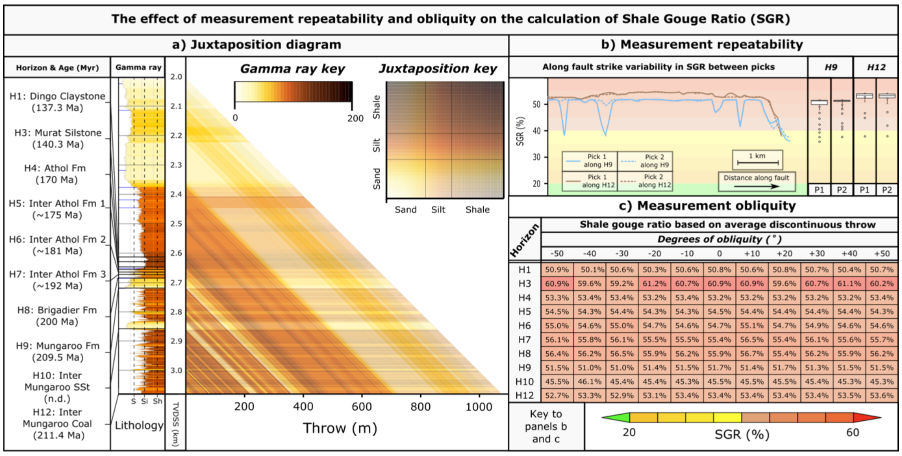

Figure 11: The effect of repeatability and obliquity on the estimation of shale gouge ratio for fault transmissivity studied. Note how for this fault all values are above the sealing threshold, and the effect of repeatability and obliquity related errors are only locally important.

Fault transmissivity is a measure of the permeability of a fault zone, and it is important to quantify for hydrocarbon exploration, CO_2 sequestration and the geological disposal of nuclear waste. A common way to assess the fault transmissivity is to calculate the shale gouge ratio (SGR, e.g., Yielding et al., 2002), which is calculated by considering the proportion of shale that has moved past a given point on a fault using the following equation:

$$SGR = \frac{\sum(V_{shale} \times \Delta z)}{throw}$$

$$(V_{shale} = proportion\ of\ shale\ in\ a\ given\ rock\ volume, \Delta z = bed\ thickness)$$

A higher SGR ratio suggests that there is a high proportion of phyllosilicates within the fault core (e.g., Foxford et al., 1998; Yielding, 2002) and a SGR of 15-20% has been suggested as a sealing limit (Yielding, 2002). We use the Chandon-1 well to calculate V_{shale} of the succession and construct a juxtaposition diagrams (Figure 11a). We calculate SGR for each point along the strike-perpendicular repeat picks of Horizons H9 and H12, and use the mean throw for obliquity datasets to compare how repeatability and obliquity errors influence the calculations.

Our assessment shows that repeatability and obliquity errors have only a minor impact on the SGR calculation for fault transmissivity (Figure 11b, c), with the V_{shale} of the intervening succession playing a more significant role in the calculation. The interval of interest between H1 and H12 is characterised by high V_{shale} values (average = 50%). As a result, most offsets exhibit siltstone-shale or shale-shale juxtapositions (Figure 11a). Despite some differences between repeat datasets, the mean values of SGR for H9 and H12 show negligible variations, with larger differences observed only locally over short distances (<500 m). Obliquity datasets also demonstrate variations in SGR between horizons, but the differences between datasets for the same horizon are low (Figure 11c). One case where the SGR may be more sensitive to uncertainties in throw is where the sandstone content of the succession is close to the SGR sealing threshold, and as such a small change in throw could push the SGR above the threshold. However, in general, repeatability and obliquity related errors can be considered insignificant when investigating fault transmissivity.

4.2 Throw and slip on faults over time using discontinuous and continuous deformation

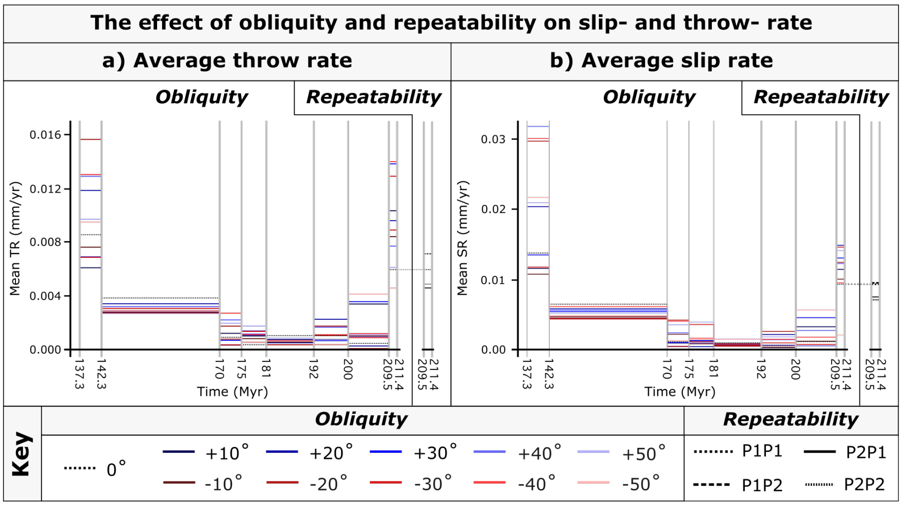

Figure 12: The effect of repeatability and obliquity on the throw- and slip- rate of SF3 over time. Obliquity errors exceed repeatability errors for both mean throw- and slip-rate, and the effect of obliquity varies between time periods. P1 and P2 relates to the first and second pick across a given horizon, with the first value relating to H12 and the latter to H9. I.e., P1P2 relates to slip rate calculated using the 1st pick across H12 and the second pick across H9.

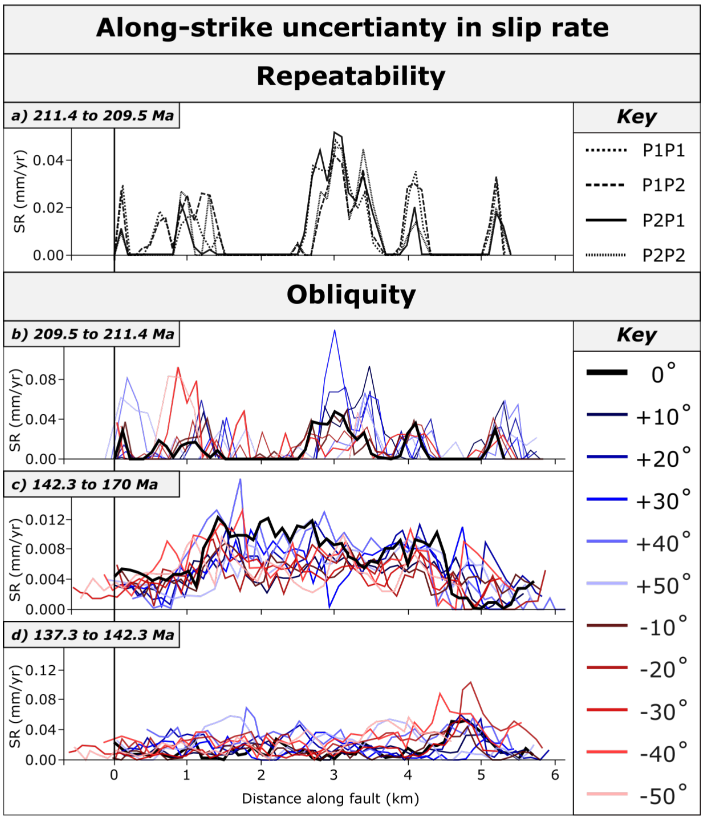

Figure 13: The effect of repeatability and obliquity on the throw- and slip- rate evolution of SF3. Note how the shape of the profile differs between time periods, and between different measurement obliquities within that time period.

When sediment accumulation rate exceeds fault throw rate, comparing the difference in throw or slip across two age-constrained horizons allows for the investigation of long-term throw or slip rate, which has applications for understanding fault growth (Marsh et al., 2010; Osagiede et al., 2014; Pan et al., 2022), strain partitioning between genetically related fault systems (Meyer et al., 2002; Cowie et al., 2005; Marsh et al., 2010) and using slip rates to understand and quantify seismic hazard (Nicol et al., 2005; Gambino et al., 2022). In our study, we focus on comparing the measurement obliquity uncertainty in throw and slip rate across SF2 using multiple age-constrained horizons. Repeat picks were limited to Horizons H9 and H12, restricting our examination of repeatability's effect on temporal slip-rate evolution, enabling the comparison of repeatability and obliquity errors for the 211.4 to 209.5 Ma period (Figure 12). Whereas uncertainties exist in the age of horizons, we do not consider these uncertainties here as they affect each dataset equally. Additionally, using the same horizon for each obliquity pick eliminates uncertainty introduced by mapping different reflections of potentially different ages.

Repeatability (211.4 to 209.5 Ma): Uncertainty in throw and slip rate, obtained from repeat picks, is influenced by the picks used and along-strike variations in fault properties (Figure 12, 13). Four pick combinations were analysed, resulting in mean throw rates ranging from 0.0045 to 0.0071 mm/yr. The percentage difference of these values (-14% to 26%) exceed the repeatability of throw extracted from continuous cut. Mean slip rates ranged from 0.0071 to 0.0095 mm/yr. Unlike throw rates, no correlation was observed between picks and mean slip rates, with the greatest difference occurring where horizon picks from the same interpretation session were used. The difference in behaviour between throw and slip rates indicates that whereas throw was consistently lower for pick 1 when compared to pick 2, the same trend does not hold for heave. Along the fault, the slip rate profile showed similar shapes for all pick combinations, but subtle differences were observed, making certain locations more susceptible to repeatability errors. Therefore, in cases with low to modest difference in slip (average 11 m) between horizons, the shape and magnitude of the slip profile may be more susceptible to repeatability errors.

Obliquity: The errors for throw and slip rates due to measurement obliquity exceed the repeatability errors for datasets (Figures 12, 13). Measurement obliquity can affect the estimates of mean throw and slip rates compared to data collected from a strike-perpendicular transect (Figure 12). From 211.4 to 209.5 Ma, throw rates extracted from oblique transects ranged from 0.0045 to 0.0140 mm/yr (absolute errors ranging from 3 to 135%), with only the -50˚ dataset having a lower throw rate than the strike-perpendicular transect. For the same time period, mean slip rates range from 0.0095 and 0.0149 mm/yr (absolute errors ranging from 1 to 60%), with all datasets (except -50°) exceeding the strike-perpendicular transect. The effect of measurement obliquity varies through time and differed between throw- and slip-rate (Figure 12). Oblique sampling resulted in over- or under-estimations of throw and slip rates, with no consistent pattern observed. Along-fault profiles were sensitive to both repeatability and obliquity errors, altering the location and magnitude of throw- and slip-rate minima and maxima (Figure 13). The influence of measurement obliquity on slip-rate profiles depended more on the time period measured (i.e., which pair of horizons were sampled) than the magnitude of measurement obliquity. Overall, even modest measurement obliquities (i.e., ±20˚), and to a lesser extent repeatability errors, led to large differences in fault length inferred from along-fault profiles and throw- or slip-rate used to calculate fault-based seismic hazard.

5. Discussion

5.1 Impact and mitigation of fault interpretation uncertainty

Interpretation repeatability

From our study, we conclude that where the quality of the seismic imagery is good and the data are extracted by an interpreter with a similar level of experience, the repeatability of extracted data will depend on the fault property being extracted, and the fault and horizon that the data is extracted from (Table 1). Throw was found to be least sensitive to repeatability errors (7%), with heave (27%), displacement (16%) and dip (16%) showing greater sensitivity. Previous work has suggested that the interpretation of fault properties from low-displacement dyke-induced faults could be affected by measurement uncertainties of between ±5% (Magee and Jackson, 2020a) and ±10% (Magee et al., 2023). Our study highlights that this range is not sufficient to capture the uncertainty in heave (and therefore displacement and dip), particularly if multiple interpreters with greater subjective bias are involved.

Suggestions: Repeatability errors are difficult to quantify and will depend on the quality of the seismic image, the experience of the interpreter, and other human factors. As such the appropriate size of the error bars will differ from the values presented in this study. However, our study provides a first-pass parametric study of the influence of repeatability errors on the extraction of fault properties, suggesting errors >10% are to be expected, particularly in low-quality datasets or where low-displacement faults are present. Study specific values could be obtained by undertaking repeat picks on a subset of the data.

Measurement Obliquity

From our study, we conclude that the derived measurement obliquity broadly follows the theoretical trends (Figure 1c), but that the magnitude of the resulting error exceeds the theoretical values. The higher than expected errors may be due to 'non-geometrical' obliquity errors of the type discussed in Section 5.2. Our findings suggest that measurement obliquity should be limited, where possible, to ±20° around the orthogonal to the local fault strike.

However, it may not be practical to always interpret orthogonal to the local fault strike, for example when only 2D seismic datasets are available, or when the fault strike is highly variable. For a fault that is highly sinuous, it would be time-consuming to construct numerous arbitrary lines orthogonal to differently orientated fault sections. In that case, additional steps would be required to ensure that the picks from differentialy orientated arbitrary lines are combined in a mathematically and geometrically appropriate way.

Suggestions: Measurement obliquity should not exceed ±20˚, and where possible ±15˚. This ensures that obliquity errors are minimised, whilst still ensuring that data is collected in a time-efficient manner. This rule is particularly important where the continuous cut-offs are measured. Where it is not possible to reduce the measurement obliquity, results could be improved by 'correcting' heave, dip, and displacement values based on local strike calculated from measured cut-offs and the theoretical relationships outlined in Figure 1c. However, whilst this would decrease the overall errors, it cannot account for any non-geometrical errors in the dataset.

Interpreted cut-off type

Our work highlights that the interpreted cut-off type influences the magnitude of both repeatability and obliquity related errors (Tables 1, S7-14, Figures 4-10). Greater uncertainty was observed where continuous cut-offs are included in the analysis, with the effect particularly clear when extracting heave (Table 1, Figure 7).

Suggestions: The choice of interpreted cut-off type is often driven by study design (e.g., whether slip-rate or fault transmusivity is important), and therefore it is limited how much this can be mitigated against. However, we found that the extraction of heave from fault cut-offs is particularly sensitive to both repeatability and obliquity errors and that the magnitude of error for the latter can greatly exceed theoretical values. Therefore, it may be better to use an average dip between two or more mapped horizons to calculate heave from the measured throw value. This will also reduce the effect of sample-specific measurement errors on the extraction of slip-rate.

5.2 Factors that control the magnitude of repeatability and non-geometrical obliquity errors.

Our study suggests that the extraction of fault properties from cut-off data is strongly affected by the three elements of fault interpretation focused on in this study, and that these elements contribute to uncertainty in deriving interpretations from these data. Additionally, the effect of each element can vary both between faults and spatially along a single fault. During the work, we identified several additional factors that combine to increase, or decrease, the uncertainty at a given point along the fault, which are summarised below and in Figure 14.

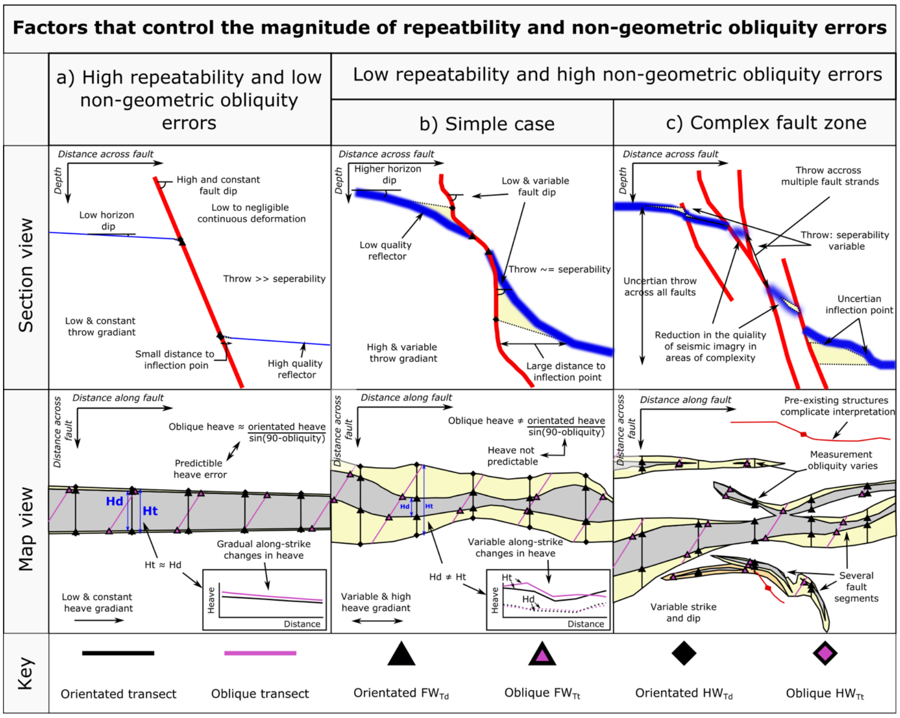

Figure 14: Cartoons showing the factors that control the repeatability and magnitude of non-geometric obliquity errors. Examples are shown for a fault with high repeatability and low geometric errors (a), low repeatability and high geometric errors (b), and a more complex fault zone that is representative of relay zones observed in the seismic cube. See text for discussion of these factors.

Our data suggests that the quality of the mapped reflection plays a large role in non-geometrical errors and low repeatability, as evidenced by certain horizons (e.g., H1) showing high errors (Table S2). Our findings thus agreed with previous studies, in that XXX (e.g., Alcalde et al., 2017; Schaaf and Bond, 2019; Chellingsworth et al., 2015*).* The effect of the reflection quality does not influence each fault property equally, with heave (and thus displacement and dip) affected more than throw, due to the low regional dip (<3˚) across the study area.

Our data shows that the uncertainty is affected by the size of the fault in terms of displacement or throw. There is greater uncertainty in areas of low throw, especially when close to or below the limit of seperability. When a large proportion of the deformation is taken up by folding (Figure 14b), uncertainties are higher due to challenges in interpreting continuous cut-offs. These challenges are related to the variability of the horizon dip, the distance to the inflection point and the variability and magnitude of fault dip. Finally, uncertainties were particularly evident in complex fault zones (Figure 14c), where the image quality may be more degraded and there may be challenges in interpreting deformation across multiple nearby fault strands. The factors shown in Figure 14 indicate why there are along-strike and down-dip variations in the uncertainties, and therefore highlights that there may be local geometric variations in fault geometry that merit additional care and quantification of uncertainties.

6. Conclusions

Our study demonstrated that fault properties extracted from seismic reflection datasets are prone to three types of uncertainty: interpretation repeatability, measurement obliquity, and interpreted cut-off type. Obliquity related errors varies depending on the horizon and fault interpreted, the magnitude of obliquity, and the fault property measured. High errors occurred when obliquity exceeded ±20˚, with throw showing lower percentage errors compared to heave across all datasets. Heave errors caused uncertainties in displacement and dip extraction, particularly in areas of low displacement. Repeatability errors were ~±10% for throw, and 13-23% for heave, with higher errors in areas of structural complexity or low seimic image quality. Measurement obliquity was not found to compound repeatability errors; however, interpreting continuous cut-offs increased uncertainty and error in extracted fault properties.

Measurement obliquity and interpretation repeatability can have a minor effect on the calculation of shale gouge ratio (SGR), but local fault plane patches showed significant errors. Average SGR values were generally insensitive to errors, but resevoirs near the sealing threashold might experience unexpected local cross-fault fluid flow, potentially affecting compliance with legislation for carbon capture and storage facilities. Slip-rate extraction, which utilises continuous cut-offs, was strongly affected by both obliquity and repeatability errors. This could lead to over- or underestimation of slip-rate and differences in the interpretated slip-rate profile. This could significantly impact fault-based seismic hazard assessments, especially in low seismicity areas, and therefore the suitability of nuclear waste disposal sites. These examples underline the importance of considering and mitigating obliquity and repeatbility errors when extracting fault data from seismic reflection datsets.

References

Alcalde, J., Bond, C.E., 2022. Chapter 5 - Subjective uncertainty and biases: The impact on seismic data interpretation. In: Bell, R., Iacopini, D., Vardy, M. (Eds.), Interpreting Subsurface Seismic Data. Elsevier, 103–123. https://doi.org/10.1016/B978-0-12-818562-9.00002-9

Alcalde, J., Bond, C.E., Johnson, G., Butler, R.W.H., Cooper, M.A., Ellis, J.F., 2017a. The importance of structural model availability on seismic interpretation. Journal of Structural Geology 97, 161–171. https://doi.org/10.1016/j.jsg.2017.03.003

Alcalde, J., Bond, C.E., Johnson, G., Ellis, J.F., Butler, R.W.H., 2017b. Impact of seismic image quality on fault interpretation uncertainty. GSA Today. https://doi.org/10.1130/GSATG282A.1

Allen, P.A., Allen, J.R., 2013. Basin Analysis: Principles and Application to Petroleum Play Assessment. John Wiley & Sons.

Amonette, J.E., Barr, J.L., Dobeck, L.M., Gullickson, K., Walsh, S.J., 2010. Spatiotemporal changes in CO2 emissions during the second ZERT injection, August–September 2008. Environmental Earth Sciences 60, 263–272. https://doi.org/10.1007/s12665-009-0402-0

Andrews, B.J., Roberts, J.J., Shipton, Z.K., Bigi, S., Tartarello, M.C., Johnson, G., 2019. How do we see fractures? Quantifying subjective bias in fracture data collection. Solid Earth 10, 487–516. https://doi.org/10.5194/se-10-487-2019

Bilal, A., McClay, K., 2022. Tectonic and stratigraphic evolution of the central Exmouth Plateau, NW Shelf of Australia. Marine and Petroleum Geology 136. https://doi.org/10.1016/j.marpetgeo.2021.105447

Bilal, A., McClay, K., Scarselli, N., 2020. Fault-scarp degradation in the central Exmouth Plateau, North West Shelf, Australia. Geological Society, London, Special Publications 476, 231–257. https://doi.org/10.1144/SP476.11

Black, M., McCormack, K.D., Elders, C., Robertson, D., 2017. Extensional fault evolution within the Exmouth Sub-basin, North West Shelf, Australia. Marine and Petroleum Geology 85, 301–315. https://doi.org/10.1016/j.marpetgeo.2017.05.022

Bond, C.E., 2015. Uncertainty in structural interpretation: Lessons to be learnt. Journal of Structural Geology 74, 185–200. https://doi.org/10.1016/j.jsg.2015.03.003

Bond, C.E., Gibbs, A.D., Shipton, Z.K., Jones, S., 2007. What do you think this is? “Conceptual uncertainty” in geoscience interpretation. GSA Today 17, 4. https://doi.org/10.1130/GSAT01711A.1

Bond, C.E., Lunn, R.J., Shipton, Z.K., Lunn, A.D., 2012. What makes an expert effective at interpreting seismic images? Geology 40, 75–78. https://doi.org/10.1130/G32375.1

Brown, A.R., 2011. Interpretation of Three-Dimensional Seismic Data, 7th ed. American Association of Petroleum Geologists.

Chellingsworth, L., Bentley, M., Wynn, T., 2015. Human factors in seismic uncertainty — Restoring a realistic uncertainty range. Interpretation 3, SQ21–SQ32. https://doi.org/10.1190/INT-2014-0203.1

Childs, C., Manzocchi, T., Nicol, A., Walsh, J.J., Soden, A.M., Conneally, J.C., Delogkos, E., 2017. The relationship between normal drag, relay ramp aspect ratio and fault zone structure. Geological Society, London, Special Publications 439, 355–372. https://doi.org/10.1144/SP439.16

Childs, C., Manzocchi, T., Walsh, J.J., Bonson, C.G., Nicol, A., Schöpfer, M.P.J., 2009. A geometric model of fault zone and fault rock thickness variations. Journal of Structural Geology 31, 117–127. https://doi.org/10.1016/j.jsg.2008.08.009

Choi, J.-H., Edwards, P., Ko, K., Kim, Y.-S., 2016. Definition and classification of fault damage zones: A review and a new methodological approach. Earth-Science Reviews 152, 70–87. https://doi.org/10.1016/j.earscirev.2015.11.006

Connor, C.B., Chapman, N.A., Connor, L.J., 2009. Volcanic and Tectonic Hazard Assessment for Nuclear Facilities. Cambridge University Press.

Cowie, P.A., Underhill, J.R., Behn, M.D., Lin, J., Gill, C.E., 2005. Spatio-temporal evolution of strain accumulation derived from multi-scale observations of Late Jurassic rifting in the northern North Sea: A critical test of models for lithospheric extension. Earth and Planetary Science Letters 234, 401–419. https://doi.org/10.1016/j.epsl.2005.01.039

Delogkos, E., Manzocchi, T., Childs, C., Sachanidis, C., Barbas, T., Schöpfer, M.P.J., Chatzipetros, A., Pavlides, S., Walsh, J.J., 2017. Throw partitioning across normal fault zones in the Ptolemais Basin, Greece. Geological Society, London, Special Publications 439, 333–353. https://doi.org/10.1144/SP439.19

Delogkos, E., Saqab, M.M., Walsh, J.J., Roche, V., Childs, C., 2020. Throw variations and strain partitioning associated with fault-bend folding along normal faults. Solid Earth 11, 935–945. https://doi.org/10.5194/se-11-935-2020

Direen, N.G., Stagg, H.M.J., Symonds, P.A., Colwell, J.B., 2008. Architecture of volcanic rifted margins: new insights from the Exmouth – Gascoyne margin, Western Australia. Australian Journal of Earth Sciences 55, 341–363. https://doi.org/10.1080/08120090701769472

Faleide, T.S., Braathen, A., Lecomte, I., Mulrooney, M.J., Midtkandal, I., Bugge, A.J., Planke, S., 2021. Impacts of seismic resolution on fault interpretation: Insights from seismic modelling. Tectonophysics 816, 229008. https://doi.org/10.1016/j.tecto.2021.229008

Fenton, C.H., Adams, J., Halchuk, S., 2006. Seismic Hazards Assessment for Radioactive Waste Disposal Sites in Regions of Low Seismic Activity. Geotechnical & Geological Engineering 24, 579–592. https://doi.org/10.1007/s10706-005-1148-4

Frodeman, R., 1995. Geological reasoning: Geology as an interpretive and historical science. Geological Society of America Bulletin 107, 960–0968. https://doi.org/10.1130/0016-7606(1995)107<0960:GRGAAI>2.3.CO;2

Gambino, S., Barreca, G., Gross, F., Monaco, C., Gutscher, M.-A., Alsop, G.I., 2022. Assessing the rate of crustal extension by 2D sequential restoration analysis: A case study from the active portion of the Malta Escarpment. Basin Research 34, 321–341. https://doi.org/10.1111/bre.12621

Gartrell, A., Torres, J., Dixon, M., Keep, M., Gartrell, A., Torres, J., Dixon, M., Keep, M., 2016. Mesozoic rift onset and its impact on the sequence stratigraphic architecture of the Northern Carnarvon Basin. The APPEA Journal 56, 143–158. https://doi.org/10.1071/AJ15012

Gibson, R.G., Bentham, P.A., 2003. Use of fault-seal analysis in understanding petroleum migration in a complexly faulted anticlinal trap, Columbus Basin, offshore Trinidad. AAPG Bulletin 87, 465–478. https://doi.org/10.1306/08010201132

Goodman, S.N., 2016. Aligning statistical and scientific reasoning. Science 352, 1180–1181. https://doi.org/10.1126/science.aaf5406

IPCC, 2005. Carbon Dioxide Capture and Storage. Cambridge University Press, Cambridge, UK.

Jackson, C.A.-L., Rotevatn, A., 2013. 3D seismic analysis of the structure and evolution of a salt-influenced normal fault zone: A test of competing fault growth models. Journal of Structural Geology 54, 215–234. https://doi.org/10.1016/j.jsg.2013.06.012

Karner, G.D., Driscoll, N.W., 1999. Style, timing and distribution of tectonic deformation across the Exmouth Plateau, northwest Australia, determined from stratal architecture and quantitative basin modelling. In: MacNiocall, C., Ryan, P. (Eds.), Continental Tectonics, Proceedings of the Ocean Drilling Program. Geological Society of London, London, UK, 271–311. https://doi.org/10.2973/odp.proc.sr.122.1992

Klusman, R.W., 2003. A geochemical perspective and assessment of leakage potential for a mature carbon dioxide–enhanced oil recovery project and as a prototype for carbon dioxide sequestration; Rangely field, Colorado. AAPG Bulletin 87, 1485–1507. https://doi.org/10.1306/04220302032

Lathrop, B.A., Jackson, C.A.-L., Bell, R.E., Rotevatn, A., 2021. Normal Fault Kinematics and the Role of Lateral Tip Retreat: An Example From Offshore NW Australia. Tectonics 40, e2020TC006631. https://doi.org/10.1029/2020TC006631

Magee, C., Jackson, C.A.-L., 2020a. Can we relate the surface expression of dike-induced normal faults to subsurface dike geometry? Geology 49, 366–371. https://doi.org/10.1130/G48171.1

Magee, C., Jackson, C.A.-L., 2020b. Seismic reflection data reveal the 3D structure of the newly discovered Exmouth Dyke Swarm, offshore NW Australia. Solid Earth 11, 579–606. https://doi.org/10.5194/se-11-579-2020

Magee, C., Love, V., Fayez, K., Andrews, B., Rivas-Dorado, S., Jackson, C., Orlov, C., Bramham, E., 2023. Quantifying Dyke-Induced Graben and Dyke Structure Using 3D Seismic Reflection Data and The Role of Interpretation Bias. Тектоніка 1, 32–53. https://doi.org/10.55575/tektonika2023.1.2.25

Magee, C., Love, V., Fayez, K., Andrews, B., Rivas-Dorado, S., Jackson, C.A.-L., Orlov, C., Bramham, E.K., in review. Quantifying dyke-induced graben and dyke structure using 3D seismic reflection data. Тектоніка.

Marsh, N., Imber, J., Holdsworth, R.E., Brockbank, P., Ringrose, P., 2010. The structural evolution of the Halten Terrace, offshore Mid-Norway: extensional fault growth and strain localisation in a multi-layer brittle–ductile system. Basin Research 22, 195–214. https://doi.org/10.1111/j.1365-2117.2009.00404.x

Meyer, V., Nicol, A., Childs, C., Walsh, J.J., Watterson, J., 2002. Progressive localisation of strain during the evolution of a normal fault population. Journal of Structural Geology 24, 1215–1231. https://doi.org/10.1016/S0191-8141(01)00104-3

Michie, E.A.H., Mulrooney, M.J., Braathen, A., 2021. Fault Interpretation Uncertainties using Seismic Data, and the Effectson Fault Seal Analysis: A Case Study from the Horda Platform, withImplications for CO₂ storage. preprint. Tectonic plate interactions, magma genesis, and lithosphere deformation at all scales/Structural geology and tectonics, rock physics, experimental deformation/Structural geology. https://doi.org/10.5194/se-2021-23

Miocic, J.M., Johnson, G., Gilfillan, S.M.V., 2014. Fault seal analysis of a natural CO2 reservoir in the Southern North Sea. Energy Procedia, 12th International Conference on Greenhouse Gas Control Technologies, GHGT-12 63, 3364–3370. https://doi.org/10.1016/j.egypro.2014.11.365

Mörner, N.-A., 2013. Patterns in seismology and palaeoseismology, and their application in long-term hazard assessments – the Swedish case in view of nuclear waste management. Pattern Recognition in Physics 1, 75–89. https://doi.org/10.5194/prp-1-75-2013

Nicol, A., Walsh, J., Berryman, K., Nodder, S., 2005. Growth of a normal fault by the accumulation of slip over millions of years. Journal of Structural Geology 27, 327–342. https://doi.org/10.1016/j.jsg.2004.09.002

Osagiede, E.E., Duffy, O.B., Jackson, C.A.-L., Wrona, T., 2014. Quantifying the growth history of seismically imaged normal faults. Journal of Structural Geology 66, 382–399. https://doi.org/10.1016/j.jsg.2014.05.021

Pan, S., Bell, R.E., Jackson, C.A.-L., Naliboff, J., 2021. Evolution of normal fault displacement and length as continental lithosphere stretches. Basin Research 34, 121–140. https://doi.org/10.1111/bre.12613

Pan, S., Naliboff, J., Bell, R., Jackson, C., 2022. Bridging Spatiotemporal Scales of Normal Fault Growth During Continental Extension Using High-Resolution 3D Numerical Models. Geochemistry, Geophysics, Geosystems 23, e2021GC010316. https://doi.org/10.1029/2021GC010316

Paumard, V., Bourget, J., Payenberg, T., Ainsworth, R.B., George, A.D., Lang, S., Posamentier, H.W., Peyrot, D., 2018. Controls on shelf-margin architecture and sediment partitioning during a syn-rift to post-rift transition: Insights from the Barrow Group (Northern Carnarvon Basin, North West Shelf, Australia). Earth-Science Reviews 177, 643–677. https://doi.org/10.1016/j.earscirev.2017.11.026

Pérez-Díaz, L., Alcalde, J., Bond, C.E., 2020. Introduction: Handling uncertainty in the geosciences: identification, mitigation and communication. Solid Earth 11, 889–897. https://doi.org/10.5194/se-11-889-2020

Reeve, M.T., Jackson, C.A.-L., Bell, R.E., Magee, C., Bastow, I.D., 2016. The stratigraphic record of prebreakup geodynamics: Evidence from the Barrow Delta, offshore Northwest Australia. Tectonics 35, 1935–1968. https://doi.org/10.1002/2016TC004172

Reeve, M.T., Magee, C., Bastow, I.D., McDermott, C., Jackson, C.A.-L., Bell, R.E., Prytulak, J., 2021. Nature of the Cuvier Abyssal Plain crust, offshore NW Australia. Journal of the Geological Society 178, jgs2020-172. https://doi.org/10.1144/jgs2020-172

Robb, M.S., Taylor, B., Goodliffe, A.M., 2005. Re-examination of the magnetic lineations of the Gascoyne and Cuvier Abyssal Plains, off NW Australia. Geophysical Journal International 163, 42–55. https://doi.org/10.1111/j.1365-246X.2005.02727.x

Robledo Carvajal, F., Butler, R.W.H., Bond, C.E., 2023. Mapping faults in 3D seismic data – why the method matters. Journal of Structural Geology 104976. https://doi.org/10.1016/j.jsg.2023.104976

Roche, V., Camanni, G., Childs, C., Manzocchi, T., Walsh, J., Conneally, J., Saqab, M.M., Delogkos, E., 2021. Variability in the three-dimensional geometry of segmented normal fault surfaces. Earth-Science Reviews 216, 103523. https://doi.org/10.1016/j.earscirev.2021.103523

Rodríguez-Salgado, P., Childs, C., Shannon, P.M., Walsh, J.J., 2023. Influence of basement fabrics on fault reactivation during rifting and inversion: a case study from the Celtic Sea basins, offshore Ireland. Journal of the Geological Society 180, jgs2022-024. https://doi.org/10.1144/jgs2022-024

Schaaf, A., Bond, C.E., 2019. Quantification of uncertainty in 3-D seismic interpretation: implications for deterministic and stochastic geomodeling and machine learning. Solid Earth 10, 1049–1061. https://doi.org/10.5194/se-10-1049-2019

Shipton, Z.K., Cowie, P.A., 2003. A conceptual model for the origin of fault damage zone structures in high-porosity sandstone. Journal of Structural Geology 25, 333–344. https://doi.org/10.1016/S0191-8141(02)00037-8

Shipton, Z.K., Roberts, J.J., Comrie, E.L., Kremer, Y., Lunn, R.J., Caine, J.S., 2020. Fault fictions: systematic biases in the conceptualization of fault-zone architecture. Geological Society, London, Special Publications 496, 125–143. https://doi.org/10.1144/SP496-2018-161

Stagg, H., Alcock, M., Bernardel, G., Moore, A., Symonds, P., Exon, N., 2004. Geological framework of the outer Exmouth Plateau and adjacent ocean basins. Geoscience Australia.

Steventon, M.J., Jackson, C.A.-L., Hall, M., Ireland, M.T., Munafo, M., Roberts, K.J., 2022. Reproducibility in Subsurface Geoscience. Earth Science, Systems and Society 2, 10051. https://doi.org/10.3389/esss.2022.10051

Tannert, C., Elvers, H.-D., Jandrig, B., 2007. The ethics of uncertainty. EMBO Reports 8, 885–974. https://doi.org/10.1038/sj.embor.7401072

Taylor, S.K., Nicol, A., Walsh, J.J., 2008. Displacement loss on growth faults due to sediment compaction. Journal of Structural Geology 30, 394–405. https://doi.org/10.1016/j.jsg.2007.11.006

Terzaghi, R.D., 1965. Sources of Error in Joint Surveys. Géotechnique 15, 287–304. https://doi.org/10.1680/geot.1965.15.3.287

Tindale, K., Newell, N., Keall, J., Smith, N., 1998. Abstract: Structural Evolution and Charge History of the Exmouth Sub-Basin Northern Carnarvon Basin, Offshore Western Australia.

Watkins, H., Bond, C.E., Healy, D., Butler, R.W.H., 2015. Appraisal of fracture sampling methods and a new workflow to characterise heterogeneous fracture networks at outcrop. Journal of Structural Geology 72, 67–82. https://doi.org/10.1016/j.jsg.2015.02.001

Yang, X.-M., Elders, C., 2016. The Mesozoic structural evolution of the Gorgon Platform, North Carnarvon Basin, Australia. Australian Journal of Earth Sciences 63, 755–770. https://doi.org/10.1080/08120099.2016.1243579

Yielding, G., 2002. Shale Gouge Ratio — calibration by geohistory. In: Koestler, A.G., Hunsdale, R. (Eds.), Norwegian Petroleum Society Special Publications, Hydrocarbon Seal Quantification. Elsevier, 1–15. https://doi.org/10.1016/S0928-8937(02)80003-0

Yielding, G., Lykakis, N., Underhill, J.R., 2011. The role of stratigraphic juxtaposition for seal integrity in proven CO2 fault-bound traps of the Southern North Sea. Petroleum Geoscience 17, 193–203. https://doi.org/10.1144/1354-0793/10-026

1064 **Supplementary data**

1065 **Supplementary 1 : data tables**

1066 ***S1.1 Repeatability statistics***

1067

Parameter	SF2				SF3				SF4				SF5				All faults			
	Equivalent datasets	% equivalent datasets	Mean Abs difference	% Absolute difference	Equivalent datasets	% equivalent datasets	Mean Abs difference	% Absolute difference	Equivalent datasets	% equivalent datasets	Mean Abs difference	% Absolute difference	Equivalent datasets	% equivalent datasets	Mean Abs difference	% Absolute difference	Equivalent datasets	% equivalent datasets	Mean Abs difference	% Absolute difference
Td: HDF 1					9	82%	7.9	7%	9	82%	5.5	8%	7	64%	1.7	6%	25	76%	5.0	7%
Td: HDF 0.1					11	100%	3.2	2%	10	91%	4.7	6%	9	82%	1	3%	30	91%	3.0	4%
Td					*20*	*91%*	*5.55*	*5%*	*19*	*86%*	*5.1*	*7%*	*16*	*73%*	*1.35*	*5%*	*55*	*83%*	*4.0*	*5%*
Tt: HDF 1	3	27%	1.8	14%	8	73%	13.1	7%	10	91%	5.6	5%	2	18%	4.3	9%	23	52%	6.2	9%
Tt: HDF 0.1	3	27%	2	16%	6	55%	12.7	6%	4	36%	5.9	6%	2	18%	2.7	6%	15	34%	5.8	9%
Tt	*6*	*27%*	*1.9*	*15%*	*14*	*64%*	*12.9*	*7%*	*14*	*64%*	*5.75*	*6%*	*14*	*64%*	*3.5*	*8%*	*48*	*55%*	*6.0*	*9%*
Throw	***6***	***27%***	***1.9***	***15%***	***34***	***77%***	***9.2***	***6%***	***33***	***75%***	***5.4***	***6%***	***30***	***68%***	***2.425***	***6%***	***103***	***69%***	***5.0***	***7%***
Hd: HDF 1					0	0%	30.0	26%	0	0%	26.5	37%	3	27%	13.2	52%	3	9%	23.2	38%
Hd: HDF 0.1					9	82%	10.8	7%	5	45%	22.5	19%	5	45%	11.1	25%	19	58%	14.8	17%
Hd					*9*	*41%*	*20.4*	*17%*	*5*	*23%*	*24.5*	*28%*	*8*	*36%*	*12.15*	*39%*	*22*	*33%*	*19.0*	*28%*
Ht: HDF 1	2	18%	8.9	42%	7	64%	25	12%	2	18%	31.1	37%	2	18%	12.3	33%	13	30%	19.3	31%
Ht: HDF 0.1	4	36%	8.6	41%	8	73%	14.1	9%	5	45%	20.1	16%	6	55%	12	19%	23	52%	13.7	21%
Ht	*6*	*27%*	*8.8*	*42%*	*15*	*68%*	*19.6*	*11%*	*7*	*32%*	*25.6*	*27%*	*8*	*36%*	*12.2*	*26%*	*36*	*41%*	*16.5*	*26%*
Heave	***6***	***27%***	***8.8***	***42%***	***24***	***55%***	***20.0***	***14%***	***12***	***27%***	***25.1***	***27%***	***16***	***36%***	***12.2***	***32%***	***58***	***37%***	***17.8***	***27%***
Dd: HDF 1					0	0%	27.1	16%	3	27%	21.9	21%	4	36%	10.7	29%	7	21%	19.9	22%
Dd: HDF 0.1					10	91%	10.1	4%	9	82%	22	15%	6	55%	8.6	15%	25	76%	13.6	11%
Dd					*10*	*45%*	*18.6*	*10%*	*12*	*55%*	*21.95*	*18%*	*8*	*36%*	*9.65*	*22%*	*30*	*45%*	*16.7*	*17%*
Dt: HDF 1	2	18%	8.7	34%	5	45%	26.2	9%	4	36%	14	9%	5	45%	7.5	12%	16	36%	14.1	16%
Dt: HDF 0.1	4	36%	7.1	27%	8	73%	17.4	7%	6	55%	21.5	13%	8	73%	7.8	10%	26	59%	13.5	14%
Dt	*6*	*27%*	*7.9*	*31%*	*13*	*59%*	*21.8*	*8%*	*10*	*45%*	*17.8*	*11%*	*13*	*59%*	*7.7*	*11%*	*42*	*48%*	*13.8*	*15%*
Displacement	***6***	***27%***	***7.9***	***31%***	***36***	***52%***	***20.2***	***9%***	***32***	***50%***	***19.9***	***15%***	***21***	***48%***	***8.7***	***17%***	***72***	***47%***	***15.3***	***16%***
Dipd: HDF 1					0	0%	5.2	12%	0	0%	9.3	*20%*	3	27%	12.9	27%	3	9%	9.1	20%
Dipd: HDF 0.1					8	73%	2.1	4%	3	27%	4	*11%*	6	55%	6.4	18%	17	52%	4.2	11%
Dipd					8	36%	*3.65*	8%	3	*14%*	*6.65*	*16%*	9	*41%*	*9.65*	*23%*	20	30%	6.7	15%
Dipt: HDF 1	4	36%	9.9	28%	1	9%	4.7	10%	0	0%	9.2	19%	4	36%	8.7	17%	9	20%	8.1	19%
Dipt: HDF 0.1	5	45%	8.4	25%	8	73%	2.1	4%	4	36%	2.8	7%	4	36%	5.8	16%	21	48%	4.8	13%
Dipt	*9*	*41%*	*9.2*	*27%*	9	41%	*3.4*	*7%*	4	*18%*	*6.0*	*13%*	8	*36%*	*7.3*	*17%*	30	34%	6.5	16%
Dip	***9***	***41%***	***9.2***	***27%***	***17***	***39%***	***3.5***	***8%***	***7***	***16%***	***6.3***	***14%***	***17***	***39%***	***8.5***	***20%***	***50***	***32%***	***6.6***	***16%***
All Discontinuous Parameters: HDF 1					9	20%		15%	12	27%		22%	17	39%		29%	38	29%		22%
All Discontinuous Parameters: HDF 0.1					38	86%		4%	27	61%		13%	26	59%		15%	91	69%		11%
All Discontinuous Parameters					47	53%		10%	39	44%		17%	41	47%		22%	127	48%		16%
Continuous: HDF 1	11	25%		30%	21	48%		10%	16	36%		18%	13	30%		18%	61	35%		19%
Continuous: HDF 0.1	16	36%		27%	30	68%		7%	19	43%		11%	20	45%		13%	85	48%		14%
Continuous	*27*	31%		28%	*51*	58%		8%	*35*	40%		14%	*43*	49%		15%	*156*	44%		16%
Average: All parameters	***27***	***31%***		***28%***	***111***	***56%***		***9%***	***84***	***42%***		***16%***	***84***	***48%***		***19%***	***283***	***46.2%***		***16%***

1068 *Table S1: Repeatability statistics*

1069

1070 ***S1.2 Obliquity statistics***

1071

Horizon	Td		Hd		Dipd		Dispd		Tt		Ht		Dipt		Dispt		Overall		Discontinuous parameters		Continuous parameters	
	% difference	% equal datasets	% difference	% equal datasets	% difference	% equal datasets	% difference	% equal datasets	% difference	% equal datasets	% difference	% equal datasets	% difference	% equal datasets	% difference	% equal datasets	% difference	% equal datasets	% difference	% equal datasets	% difference	% equal datasets
H1	13%	60%	32%	40%	13%	35%	22%	50%	20%	50%	52%	47%	18%	47%	30%	57%	26%	49%	20%	46%	30%	50%
H2	11%	87%	31%	70%	14%	57%	22%	77%	13%	70%	65%	28%	19%	28%	43%	33%	28%	54%	19%	73%	35%	39%
H3	6%	97%	20%	73%	11%	53%	14%	77%	12%	65%	25%	55%	12%	38%	18%	63%	5%	63%	13%	75%	17%	54%
H4	6%	87%	25%	57%	12%	50%	16%	70%	16%	75%	28%	50%	1%	43%	18%	58%	16%	60%	15%	65%	16%	56%
H5	5%	90%	26%	45%	11%	40%	18%	45%	6%	73%	34%	100%	13%	40%	20%	57%	17%	53%	15%	55%	18%	52%
H6	6%	97%	25%	57%	12%	43%	16%	70%	6%	85%	37%	45%	14%	40%	22%	60%	17%	61%	15%	67%	20%	58%
H7	6%	97%	26%	57%	11%	50%	13%	73%	8%	80%	49%	28%	18%	18%	21%	58%	20%	56%	14%	69%	24%	46%
TM	4%	100%	44%	50%	14%	33%	15%	73%	7%	90%	34%	40%	27%	45%	16%	70%	18%	63%	19%	64%	17%	61%
H8	5%	97%	29%	47%	12%	33%	17%	63%	11%	78%	39%	45%	15%	30%	25%	43%	20%	54%	16%	60%	23%	49%
H9	1%	100%	53%	20%	25%	10%	28%	20%	7%	70%	42%	30%	17%	30%	25%	40%	24%	41%	27%	38%	23%	43%
IMC	8%	100%	37%	33%	15%	37%	23%	47%	10%	75%	35%	43%	13%	38%	22%	53%	20%	53%	21%	54%	20%	52%
H10a	13%	80%	23%	80%	14%	50%	12%	90%	12%	90%	37%	60%	15%	50%	20%	70%	18%	71%	15%	75%	21%	68%
H11	8%	80%	34%	50%	13%	40%	14%	55%	6%	100%	40%	30%	14%	20%	16%	60%	18%	54%	17%	56%	19%	53%
H12	4%	100%	25%	70%	10%	40%	13%	80%	5%	100%	66%	10%	25%	10%	36%	20%	23%	54%	13%	73%	33%	35%
H14	8%	90%	38%	55%	12%	45%	11%	70%	9%	70%	64%	30%	20%	20%	25%	40%	23%	54%	17%	65%	30%	40%
Total	**7%**	**91%**	**31%**	**54%**	**13%**	**43%**	**17%**	**65%**	**10%**	**76%**	**41%**	**40%**	**15%**	**34%**	**15%**	**53%**	**20%**	**56%**	**17%**	63%	**22%**	51%

1072 **Table S2: Obliquity statistics split by the horizon the data is collected from.**

Obliquity	SF2			SF3			SF4			SF5			ALL FAULTS		
	Abs difference	% difference	% equal datasets	Abs difference	% difference	% equal datasets	Abs difference	% difference	% equal datasets	Abs difference	% difference	% equal datasets	mean abs difference	% difference	% equal datasets
-50	2.95	24%	36%	9.19	7%	83%	4.79	6%	92%	5.87	18%	75%	6.11	12%	78%
-40	1.92	15%	55%	12.39	10%	58%	4.87	6%	92%	3.4	11%	90%	6.33	10%	77%
-30	1.86	14%	64%	9.65	9%	58%	2.98	4%	88%	2.86	9%	95%	4.77	8%	78%
-20	0.69	6%	100%	10.02	8%	83%	3.11	4%	100%	2.83	9%	95%	4.76	7%	94%
-10	0.77	6%	91%	5.52	5%	88%	2.69	4%	92%	2.35	7%	100%	3.18	5%	93%
10	1.2	10%	82%	10.86	9%	54%	2.16	3%	100%	3.06	10%	85%	4.83	7%	80%
20	1.61	13%	64%	5.19	5%	92%	2.56	3%	92%	3.15	9%	90%	3.36	6%	88%
30	0.72	16%	55%	10.01	9%	63%	3.61	4%	92%	4.2	12%	95%	5.42	9%	79%
40	1.64	13%	64%	9.1	7%	79%	4.07	5%	92%	3.99	12%	95%	5.22	8%	85%
50	1.86	15%	64%	14.08	14%	75%	8.06	10%	73%	4.41	13%	95%	8.1	13%	78%
Total	**1.64**	**13%**	**67%**	**9.6**	**8%**	**73%**	**3.89**	**5%**	**92%**	**3.61**	**11%**	**92%**	**5.21**	**9%**	**83%**

Table S3: Obliquity statistics for Throw

Obliquity	SF2			SF3			SF4			SF5			ALL FAULTS		
	Abs difference	% difference	% equal datasets	Abs difference	% difference	% equal datasets	Abs difference	% difference	% equal datasets	Abs difference	% difference	% equal datasets	mean abs difference	% difference	% equal datasets
-50	15.01	128%	18%	64.51	55%	13%	60.69	76%	8%	20.37	65%	45%	45.66	74%	20%
-40	5.45	45%	27%	61.78	49%	4%	40.62	51%	19%	12.01	40%	55%	35.05	47%	25%
-30	2.72	24%	45%	30.31	25%	29%	26.08	33%	38%	7.35	26%	75%	19.54	28%	46%
-20	2.65	24%	27%	17.69	15%	67%	10.36	13%	69%	5.09	18%	85%	10.18	16%	67%
-10	3.16	29%	82%	8.86	7%	79%	4.34	6%	96%	4.59	15%	95%	5.58	12%	89%
10	2.06	20%	82%	18.83	17%	54%	13.6	18%	54%	4.76	16%	90%	11.4	18%	67%
20	3.43	32%	64%	10.13	9%	88%	17.09	22%	46%	5.73	23%	80%	10.37	20%	69%
30	7.32	69%	36%	30.29	27%	21%	23.5	30%	19%	8.4	32%	85%	19.59	35%	38%
40	4.3	37%	45%	52.59	42%	4%	37.15	48%	8%	12.69	55%	45%	31.22	46%	21%
50	9.77	83%	9%	97.07	79%	8%	65.75	82%	8%	12.39	44%	45%	54.25	72%	17%
Total	**5.59**	**49%**	**44%**	**39.21**	**33%**	**37%**	**29.92**	**38%**	**37%**	**9.34**	**33%**	**70%**	**24.28**	**37%**	**46%**

Table S4: Obliquity statistics for Heave

Obliquity	SF2			SF3			SF4			SF5			ALL FAULTS		
	Abs difference	% difference	% equal datasets	Abs difference	% difference	% equal datasets	Abs difference	% difference	% equal datasets	Abs difference	% difference	% equal datasets	mean abs difference	% difference	% equal datasets
-50	15.56	88%	9%	51.03	28%	17%	48.78	41%	15%	19.29	41%	50%	37.65	44%	23%
-40	4.84	27%	55%	54.65	28%	8%	33.74	28%	31%	10.41	23%	65%	30.25	27%	36%
-30	3	17%	73%	27.03	16%	33%	20.28	17%	50%	7.27	17%	80%	16.72	17%	56%
-20	1.89	11%	91%	19.88	11%	71%	8.76	7%	77%	5.49	13%	95%	10.31	10%	81%
-10	2.76	17%	82%	10.04	6%	79%	4.14	4%	96%	4.69	10%	100%	5.84	8%	90%
10	1.34	8%	91%	17.53	10%	58%	10.47	9%	62%	4.62	10%	95%	9.88	10%	73%
20	2.27	13%	91%	10.29	6%	83%	13.94	12%	54%	5.32	12%	95%	9.15	11%	78%
30	5.6	34%	45%	24.51	14%	50%	19.61	17%	54%	7.05	16%	95%	16.06	18%	62%
40	3.27	18%	73%	43.68	23%	33%	30.37	27%	23%	8.75	24%	85%	25.25	24%	48%
50	7.72	43%	45%	81.3	44%	8%	55.81	48%	8%	8.34	19%	95%	45.11	39%	35%
Total	**4.38**	**28%**	**65%**	**34**	**19%**	**44%**	**24.59**	**21%**	**47%**	**8.11**	**18%**	**86%**	**20.62**	**21%**	**58%**

Table S5: Obliquity statistics for Displacement

Obliquity	**Dip**														
	SF2			SF3			SF4			SF5			All faults		
	Abs difference	% difference	% equal datasets	Abs difference	% difference	% equal datasets	Abs difference	% difference	% equal datasets	Abs difference	% difference	% equal datasets	mean abs difference	% difference	% equal datasets
-50	8.95	18%	18%	10.09	21%	0%	13.9	29%	0%	8.41	17%	45%	10.74	22%	14%
-40	7.7	15%	45%	8.05	18%	4%	9.36	20%	8%	6.77	14%	45%	8.12	17%	21%
-30	5.5	11%	64%	4.73	10%	29%	7.03	15%	4%	3.91	8%	80%	5.37	11%	38%
-20	5.79	12%	73%	2.44	6%	67%	3.34	7%	50%	3.53	7%	75%	3.45	7%	64%
-10	5.74	12%	64%	1.73	4%	92%	1.55	3%	81%	2.71	6%	85%	2.45	5%	83%
10	6.46	13%	36%	3.17	6%	67%	4.64	10%	50%	3.41	7%	75%	4.15	8%	59%
20	9.07	18%	27%	1.95	4%	88%	4.95	10%	31%	5.5	11%	75%	4.75	10%	58%
30	11.05	22%	18%	5.14	11%	17%	6.17	13%	4%	5.81	11%	75%	6.44	13%	27%
40	7.96	16%	45%	7.2	16%	4%	9.5	20%	0%	12.19	25%	5%	9.27	19%	9%
50	15.13	30%	0%	11.95	25%	0%	13.84	29%	0%	11.53	24%	20%	12.88	27%	5%
Total	**8.33**	**16%**	**39%**	**5.64**	**12%**	**37%**	**7.43**	**16%**	**23%**	**6.38**	**13%**	**58%**	**6.76**	**14%**	**38%**

Table S6: Obliquity statistics for Dip

Obliquity	SF3		SF4		SF5		All faults	
	% er	% equal datasets	% er	% equal datasets	% er	% equal datasets	% er	% equal datasets
-50	7%	83%	8%	92%	11%	90%	9%	89%
-40	9%	75%	5%	100%	8%	100%	7%	91%
-30	10%	50%	4%	92%	10%	100%	8%	80%
-20	6%	92%	4%	100%	11%	90%	7%	94%
-10	4%	92%	3%	100%	8%	100%	6%	97%
10	9%	58%	3%	100%	12%	80%	7%	80%
20	4%	92%	2%	100%	7%	100%	4%	97%
30	8%	83%	2%	100%	11%	100%	7%	94%
40	4%	100%	4%	100%	11%	90%	6%	97%
50	7%	92%	6%	100%	17%	90%	9%	94%
Total	**7%**	**82%**	**4%**	**85%**	**11%**	**94%**	**7%**	**91%**

Table S7: Obliquity data for discontinuous throw

Obliquity	Fault								All faults	
	SF2		SF3		SF4		SF5			
	% er	% equal datasets	% er	% equal datasets	% er	% equal datasets	% er	% equal datasets	% er	% equal datasets
-50	24%	36%	6%	83%	5%	92%	24%	60%	14%	70%
-40	15%	55%	12%	42%	7%	85%	13%	80%	11%	65%
-30	14%	64%	8%	67%	4%	85%	9%	90%	9%	76%
-20	6%	100%	10%	75%	4%	100%	8%	100%	7%	93%
-10	6%	91%	4%	83%	4%	85%	7%	100%	5%	89%
10	10%	82%	9%	50%	3%	100%	7%	90%	7%	80%
20	13%	64%	6%	92%	4%	85%	10%	80%	8%	80%
30	16%	55%	9%	42%	6%	85%	13%	90%	11%	67%
40	13%	64%	10%	58%	7%	85%	13%	100%	10%	76%
50	15%	64%	21%	58%	14%	46%	10%	100%	15%	65%
Total	**13%**	**67%**	**9%**	**65%**	**6%**	**85%**	**11%**	**89%**	**11%**	**76%**

Table S8: Obliquity data for total throw

Obliquity	SF3		SF4		SF5		All faults	
	% er	% equal datasets	% er	% equal datasets	% er	% equal datasets	% er	% equal datasets
-50	61%	17%	60%	15%	45%	70%	56%	2%
-40	46%	8%	37%	23%	34%	70%	39%	24%
-30	29%	25%	22%	77%	22%	90%	24%	48%
-20	11%	83%	4%	100%	13%	100%	9%	72%
-10	8%	67%	5%	100%	13%	90%	9%	65%
10	22%	50%	10%	77%	16%	90%	16%	54%
20	10%	83%	14%	77%	23%	70%	15%	59%
30	33%	17%	25%	23%	37%	80%	31%	28%
40	39%	0%	42%	15%	70%	50%	49%	15%
50	67%	17%	60%	15%	44%	50%	58%	20%
Total	**33%**	**82%**	**28%**	**52%**	**32%**	**76%**	**31%**	**41%**

Table S9: Obliquity data for discontinuous heave

Obliquity	Fault								All faults	
	SF2		SF3		SF4		SF5			
	% er	% equal datasets	% er	% equal datasets	% er	% equal datasets	% er	% equal datasets	% er	% equal datasets
-50	128%	18%	50%	83%	92%	0%	85%	20%	88%	11%
-40	45%	27%	53%	42%	65%	15%	47%	40%	53%	20%
-30	24%	45%	22%	67%	43%	0%	29%	60%	30%	33%
-20	24%	27%	19%	75%	21%	38%	23%	70%	22%	46%
-10	29%	82%	6%	83%	6%	92%	16%	100%	14%	91%
10	20%	82%	12%	50%	26%	31%	17%	90%	19%	63%
20	32%	64%	8%	92%	30%	15%	22%	90%	23%	63%
30	69%	36%	22%	42%	34%	15%	27%	90%	38%	39%
40	37%	45%	45%	58%	53%	0%	39%	40%	44%	22%
50	83%	9%	91%	58%	104%	0%	44%	40%	83%	11%
Total	**49%**	**44%**	**33%**	**37%**	**48%**	**85%**	**35%**	**64%**	**41%**	**40%**

Table S10: Obliquity data for total heave

Obliquity	SF3		SF4		SF5		All faults	
	% er	% equal datasets	% er	% equal datasets	% er	% equal datasets	% er	% equal datasets
-50	31%	17%	31%	31%	29%	80%	31%	30%
-40	26%	8%	20%	46%	18%	80%	21%	33%
-30	18%	25%	11%	85%	15%	90%	15%	50%
-20	8%	83%	3%	100%	12%	100%	7%	72%
-10	7%	75%	4%	100%	10%	100%	7%	70%
10	12%	50%	6%	77%	11%	100%	10%	57%
20	6%	83%	8%	77%	12%	90%	8%	63%
30	17%	33%	14%	69%	17%	100%	16%	50%
40	1%	50%	24%	46%	32%	80%	25%	43%
50	33%	17%	34%	15%	19%	90%	29%	28%
All obliquities	**18%**	**44%**	**16%**	**65%**	**17%**	**91%**	**17%**	**50%**

Table S11: Obliquity data for discontinuous displacement

Obliquity	Fault								All faults	
	SF2		SF3		SF4		SF5			
	% er	% equal datasets	% er	% equal datasets	% er	% equal datasets	% er	% equal datasets	% er	% equal datasets
-50	88%	9%	24%	17%	51%	0%	53%	20%	53%	11%
-40	27%	55%	31%	8%	37%	15%	27%	50%	31%	30%
-30	17%	73%	14%	42%	23%	15%	18%	100%	18%	48%
-20	11%	91%	14%	58%	12%	54%	13%	90%	13%	72%
-10	17%	82%	5%	83%	4%	92%	10%	100%	9%	89%
10	8%	91%	7%	67%	13%	46%	9%	90%	9%	72%
20	13%	91%	6%	83%	16%	31%	13%	100%	12%	74%
30	34%	45%	11%	67%	20%	38%	15%	90%	20%	59%
40	18%	73%	25%	17%	30%	0%	16%	90%	23%	41%
50	43%	45%	55%	0%	62%	0%	18%	100%	46%	33%
Total	**28%**	**65%**	**19%**	**44%**	**27%**	**14%**	**19%**	**80%**	**23%**	**53%**

Table S12: Obliquity data for total displacement

Obliquity	SF3		SF4		SF5		All faults	
	% er	% equal datasets	% er	% equal datasets	% er	% equal datasets	% er	% equal datasets
-50	22%	0%	26%	0%	15%	60%	21%	13%
-40	18%	8%	16%	8%	12%	40%	39%	13%
-30	11%	17%	11%	8%	6%	90%	10%	26%
-20	6%	75%	4%	85%	7%	90%	6%	63%
-10	4%	83%	3%	85%	6%	90%	9%	65%
10	6%	75%	6%	77%	6%	90%	6%	61%
20	5%	83%	8%	46%	10%	80%	8%	52%
30	11%	8%	13%	8%	13%	80%	12%	22%
40	16%	8%	19%	0%	28%	0%	20%	2%
50	26%	0%	25%	0%	24%	30%	25%	7%
Total	**13%**	**36%**	**13%**	**52%**	**13%**	**76%**	**13%**	**32%**

Table S13: Obliquity data for discontinuous dip

Obliquity	Fault								All faults	
	SF2		SF3		SF4		SF5			
	% er	% equal datasets	% er	% equal datasets	% er	% equal datasets	% er	% equal datasets	% er	% equal datasets
-50	18%	18%	21%	0%	33%	0%	20%	30%	23%	11%
-40	37%	45%	17%	0%	24%	8%	15%	50%	18%	24%
-30	11%	64%	9%	42%	19%	0%	9%	70%	12%	41%
-20	12%	73%	5%	58%	10%	15%	7%	60%	9%	50%
-10	12%	64%	4%	100%	3%	77%	5%	80%	6%	80%
10	13%	36%	6%	58%	13%	23%	7%	60%	10%	43%
20	18%	27%	3%	92%	13%	15%	12%	70%	11%	50%
30	22%	18%	10%	25%	14%	0%	9%	70%	38%	26%
40	16%	45%	15%	0%	22%	0%	21%	10%	19%	13%
50	30%	0%	24%	0%	33%	0%	23%	10%	28%	2%
Total	**16%**	**39%**	**11%**	**37%**	**18%**	**14%**	**13%**	**64%**	**15%**	**34%**

Table S14: Obliquity data for total dip

Supplementary 2: Time-depth conversion

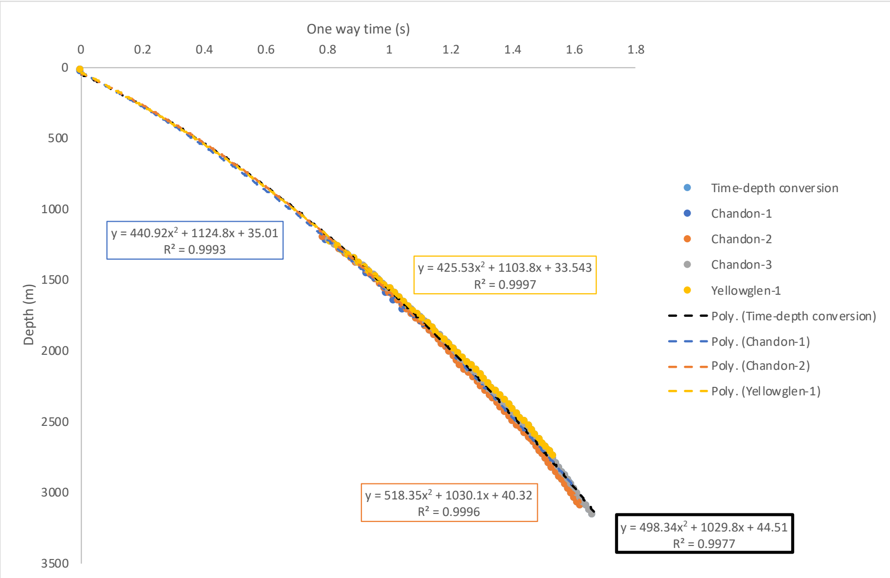

Figure S2.1: Checkshot data and best fit polynomial. The combined dataset (black) is used to convert cut-off data from time to depth.

Supplementary 8: Statistical approach used to analyse the obliquity and repeatability datasets.

Repeatability datasets:

Individual picks: The presentation of individual pick data enables us to investigate the along-strike and down-dip variability in fault parameters as well where errors differ from population values. We report the differences as $(pick\ 1 - pick\ 2)$ and hypothesise that picks undertaken at the same location on the fault should be identical; therefore, the difference between picks should be zero. To enable datasets to be compared across fault parameters we also report the % difference of individual picks (i.e., $(pick\ 1 - pick\ 2)/(\frac{pick\ 1 + pick\ 2}{2})) \times 100)$. Because the picks are independent on each other, we report differences and % difference as absolute values.

Dataset statistics: The appropriate statistical test depends on a) whether the groups are dependent on each other; and b) whether the data is normally distributed. Because repeat measurements are undertaken at the same location, they can be considered dependent. In this case, we first test whether the difference between picks for a given dataset can be considered as normally distributed using the Shapiro-Wilk's test (Shapiro and Wilk, 1965; Royston, 1995), which is widely used to test the univariate normality of populations (Thode, 2002). In this study, we use the amended version of the test which enables it to be used on datasets which range in size from 3 ≤ n ≤ 5000, with our datasets ranging from 14 to 80.

Where the null hypothesis is met for the Shapiro-Wilk test (i.e., there is a 95% probability (p-value > 0.05) that $pick\ 1 - pick\ 2$ follows a normal distribution), we calculate population statistics and undertake a paired t-test to test whether the datasets may be considered statistically equivalent. The null hypothesis for the paired t-test (H_0) is that the difference in population means between pick 1 and pick 2 are zero (i.e., the repeat picks can be considered equivalent). Because the repeat dataset may have a mean that is either higher or lower than the original pick, we use a two tailed t-test with an alternative hypothesis (H_1) of $pick\ 1\ \neq pick\ 2$. Where the alternative hypothesis is met for the Shapiro-Wilk test (i.e., there is a 95% probability (p-value < 0.05) that $pick\ 1 - pick\ 2$ does **not** follow a normal distribution), we use the Mann-Whitney U test, also termed the Wilcoxon Rank Sum Test. This is widely considered the nonparametric alternative to the 2-sample t-test. We use the same null and alternative hypothesis as the paired t-test.

Commented [ZM1]: Check that this is correct

To enable datasets to be compared based on certain parameters (e.g., obliquity, fault, horizon, measurement type), we report the average difference between population means, the average % difference, and the proportion of datasets that can be considered equivalent. An example of the latter is if 8 out of 10 horizons had a p-value greater than 0.05 for discontinuous throw, we would report that the % of datasets that can be considered equal is 80%). The reporting of aggregated dataset statistics enables parameters that have a different number of datasets (e.g., discontinuous, and continuous throw) to be directly compared.

Measurement obliquity datasets:

Individual picks: For measurement obliquity datasets, the measurement location is not located at the exact same place along the fault (Figure 1a). Therefore, where values are directly compared (e.g., strike projections), the along-strike profiles are extrapolated using a linear extrapolation and resampled to the same pick spacing. Absolute differences are not reported but used to calculate % error. For the obliquity datasets, we assume that the dataset extracted from an orthogonally orientated transect represents the 'correct' distribution. Due to the obliquity datasets not being measured at the same along-strike location, we first take the resampled datasets of both the oblique and orientated picks. We then calculate the % error for each resampled location using the following equation:

$$\left(\frac{Oblique\ pick - Orientated\ pick}{Orientated\ pick}\right) \times 100$$

Dataset statistics: The sample locations for oblique picks are not equal, and therefore the datasets cannot be considered as dependant (i.e., they are an unpaired dataset). We therefore use the Mann-Whitney U test to test whether the oblique dataset may be considered statistically equivalent to the orientated dataset (H_0) or whether they are statistically different (H_1). Similarly, to the repeatability datasets, we report the absolute difference between population mean/medians, the % difference between population mean/median and the proportion of datasets that may be considered equal for data.

Comparing interpreted deformation style datasets:

To enable the effect of deformation type to be isolated, we initially combine and discuss the obliquity and repeatability statistics of each fault parameter for each deformation type (i.e., take the average values for absolute difference, % difference, and % of equal datasets of the discontinuous and continuous datasets). Following this, we then compare discontinuous and continuous obliquity and repeatability datasets in the same manner as described above.